Reconstruction of current profiles from HF radar surface current measurements by inverse modeling

April 1991

H 972

delft hydraulics

Reconstruction of current profiles from HF radar surface current measurements by inverse modeling

C.F. de Valk

delft hydraulics

CONTENTS

ABSTRACT

A new method for reconstruction of current profiles from current measurements is described. The reconstruction is done by inversion of a model of the current profile dynamics, and can be applied in shallow tidal seas. An intended application of the method is the reconstruction of current profiles from surface current measurements obtained by HF radar. In this study, the reconstruction method was designed and implemented, and tested using data from HF radar and several other types of sensors. These data were collected in an experiment with an HF radar system, carried out in 1988 by Rijkswaterstaat (Netherlands Ministry of Transport and Public Works). Results of the tests show that, in principle, profile reconstruction works, provided reasonable estimates of water level and wind are available and the HF radar data are correct. In the tests, however, errors in the HF radar current directions were found. A procedure for validation of HF radar current data is proposed. The achievable improvement of current estimates by profile reconstruction depends on the conditions, in particular on tidal phase. Around and after the turn of the tide when the achievable improvement is most significant, reconstruction of the profile is most difficult. Therefore, the profile reconstruction method can offer a substantial improvement, provided that an accurate model of the current profile dynamics is used. Improvements of the model are proposed that will make it possible to meet the accuracy requirements. Finally, the operational feasibility of the method is discussed. The computational effort will not be restrictive for the intended application even if a more complex model of the current profile dynamics is used. This study was carried out by DELFT HYDRAULICS for Rijkswaterstaat, with financial support from the Netherlands Remote Sensing Board (BCRS project OP-1.30).

1. Introduction

1.1 Purpose of the study

HF radar is a promising new technique for simultaneous measurement of surface currents over a large area. In 1988, Rijkswaterstaat (the Netherlands Ministry of Public Works) performed an experiment with the HF radar system OSCR, provided by MAREX (Rijkswaterstaat, 1990). Current measurements with a number of different sensors and flow model simulations were performed in order to compare the HF radar data with presently available methods to obtain current data. Possible applications of an HF radar system in the Netherlands are current monitoring for prediction of transport of pollutants and sediment and for guidance of shipping traffic. Each of these applications has its specific requirements on current data. Often, the kind of data required is not surface current, but depth-averaged current, or current averaged over a certain layer, which is in general not the same. The relationship between surface current and currents at greater depths is not constant but depends on the conditions (tidal phase, wind). Therefore, in (Rijkswaterstaat, 1990), it was recommended to study this relationship in order to find out whether it is possible to reconstruct the depth-averaged current, or even the entire current profile, from surface current measurements. This is the objective of the present study.

1.2 Principle of the current profile reconstruction method

The dynamics of the current profile can be described by the shallow water equations, describing the momentum balance under the assumption of a hydrostatic pressure distribution. In this equation, terms involving horizontal gradients of surface slope and current velocity appear. A local (1DV) model can be obtained from the shallow water equations by collecting all terms involving spatial gradients in a single term, which is then replaced by its depth average, say j. So j consists of surface slope plus some additional (relatively small) terms. In the next chapter it is shown that under certain assumptions this term j can be eliminated from the model. What is left then is a model for the current velocity which requires as input data time series of the

- depth-averaged current vector
- wind vector (at given height above the surface)
- water level

plus certain parameters that are considered as fixed.

Output is the current profile as a function of time, and therefore also the surface current. If this model can be inverted somehow (that is, if from the surface current, the depth-averaged current and if necessary also other model inputs can be reconstructed), then this inverse can be used to reconstruct the entire current profile from measurements of surface current. Inversion of the model can in principle be carried out by correcting the inputs over a past time interval in such a way that the computed surface current fits the

measured surface current as good as possible. The fit can be expressed in terms of a norm of the difference between computation and measurements, and the reconstruction involves minimization of this norm by adjusting the unknown model inputs. The background of this approach is, for example, given in Chavent(1980), Luenberger(1969), Sage and Melsa(1971).

Three questions arise:

[1] Which of the model inputs (depth-averaged current, wind, water level) need to be corrected?

This depends on the accuracies of first guesses of these inputs. For the depth-averaged current, the HF radar surface current measurements can serve as a first guess. This first guess is accurate enough only if the current profile is practically uniform over the depth. In that case, the HF radar data are already sufficient and no algorithm for profile reconstruction is needed. Assuming for the moment that this is not the case, depth-averaged current will have to be corrected.
First guesses for wind can be wind analyses or predictions from the weather service or wind measurements at a nearby location. First guesses for water level can be the local astronomical tide, or real-time water level predictions. Whether wind or water level have to be corrected depends not only on the accuracies of the first guess data, but also on the sensitivity of the model to errors in these inputs.

[2] Is it possible to reconstruct the entire current profile based on surface current measurements?

This depends on structural properties of the model (in fact on a property known as observability with unknown inputs, see section 4.2), and on which inputs have to be corrected, so on the answer to 1 above. In section 4.2, it will be explained that the current profile can be reconstructed only if the first guesses of wind and water level are accurate enough and need not to be corrected. If this is not the case, it is still possible to make a statistically optimal estimate of the current profile, but the accuracy of this estimate then depends critically on the accuracies of first guesses of the model inputs.

[3] The accuracy of the reconstruction.

Shortcomings of the model will directly affect the accuracy of the reconstruction (bias or systematic error). If the model is perfect, then the accuracy of the reconstruction depends on the accuracies of the surface current measurements and of first guesses of model inputs, as well as on the sensitivities of the model.

1.3 Brief outline of the report

In the next chapter, the current profile model will be described in detail. In chapter 3, the model will be tested by comparison with measured current profiles, in order to identify shortcomings. In chapter 4, the reconstruction method will be discussed, and in particular the properties of the model that determine whether the current profile can be reconstructed from surface current data, and under what conditions (observability). In chapter 5, numerical tests will be performed with the reconstruction method, to see whether it is sufficient to only correct the depth-averaged current or whether also the water level or the wind have to be corrected. Moreover, the reconstructions are compared with field data to evaluate the method, and to identify aspects that need to be improved.

2. Modeling of current profile dynamics

Tidal flow in a shallow sea is described by the shallow water equations, based on the assumption of a hydrostatic pressure distribution. Consider a fixed local coordinate frame, with points indicated by $\mathbf{x} \triangleq (x_1, x_2, x_3)'$, with x_3 the vertical coordinate (positive upward), and x_2 the coordinate in the direction found by rotating the x_1 direction clockwise over an angle of $\pi/2$, facing the earth's surface from space.

Let ζ be the elevation of the water surface relative to some reference plane, and d the position of the bottom relative to the same reference plane. The depth h of the water column is

$$h \triangleq \zeta - d \tag{1}$$

Let $\mathbf{u} \triangleq (u_1, u_2, u_3)'$ be the velocity vector. We will consider the case that the fluid has uniform density ρ_w. For tidal flow in a shallow sea, horizontal gradients are much smaller than vertical gradients and their effect on the distribution of momentum over the water column can be neglected at a reasonable distance from the shore. Moreover, the contribution of the gradient of atmospheric pressure is negligible. In appendix a1, it is shown that under these assumptions, the horizontal components of the velocity satisfy

$$\dot{u}_i + \sum_{j=1,2} s_{ij} \gamma u_j + \mathit{j}_i - \partial/\partial x_3 \, \nu \, \partial u_i/\partial x_3 = 0 \qquad i=1,2 \tag{2a}$$

with

$$\mathit{j}_i \triangleq g \partial\zeta/\partial x_i + \text{depth averages of terms involving horizontal velocity gradients} \tag{2b}$$

and ν the eddy viscosity, γ the coriolis parameter (γ equals $2\Omega\sin(\phi)$, with ϕ the latitude, taken positive on the Northern hemisphere and negative on the Southern hemisphere, and Ω the angular velocity of the earth) and $s_{ij} = 0$ for all i,j, except $s_{12} \triangleq -1$, and $s_{21} \triangleq 1$. g is the acceleration of gravity. The boundary conditions at the water surface and at the bottom are

$$\nu_{i3} \partial u_i/\partial x_3 \Big|_{\zeta} = \tau_{s,i}/\rho_w \qquad \nu_{i3} \partial u_i/\partial x_3 \Big|_{d} = \tau_{b,i}/\rho_w \qquad i=1,2 \tag{3}$$

Now the vertical coordinate x is replaced by a scaled depth σ, which is zero at the surface and one at the bottom:

$$\sigma(x) \triangleq (\zeta - x)/h \tag{4}$$

Moreover, the horizontal velocity can be written as a number in the complex plane as

$$u \triangleq u_1 + iu_2 \tag{5}$$

(note that multiplication by i is equivalent to clockwise rotation over $\pi/2$, when facing the surface from above). Writing the stresses as complex numbers as

$$\tau_s \triangleq \tau_{s,1} + i\tau_{s,2} \qquad \tau_b \triangleq \tau_{b,1} + i\tau_{b,2} \tag{6}$$

and writing f_1 and f_2 in complex form as

$$f \triangleq f_1 + if_2 \tag{7}$$

Then (2) becomes

$$\dot{u} + i\gamma u - Lu = -f \tag{8a}$$

with L the differential operator defined by

$$L \triangleq h^{-2}\partial/\sigma\ \nu\partial/\partial\sigma \tag{8b}$$

and with boundary conditions, from (3) and (6)

$$-h^{-2}\nu\ \partial u/\partial\sigma\big|_0 = \tau_s/(\rho_w h) \qquad -h^{-2}\nu\ \partial u/\partial\sigma\big|_1 = \tau_b/(\rho_w h) \tag{8c}$$

The surface stress τ_s in (8) can be computed from the wind speed v(z) at an arbitrary height z above the surface for example by inverting the Charnok relationship which is given by

$$\tau_s = |u_*|^2\rho_a \qquad v(z) = u_*\kappa^{-1}\ \ln(z/z_0) \qquad z_0 = 0.0144|u_*^2|/g \tag{8d}$$

with κ a constant. (8) can now be solved if formulations for bottom stress τ_b and eddy viscosity ν are added.
If (8) is used for the purpose of reconstructing current profiles from surface current data, f will be among the model inputs to be reconstructed. Then a

first guess of j has to be specified based on available data, such as HF surface current data. To generate this first guess for j, the dynamics can be ignored (which in very shallow water is a good approximation anyway) and the surface current can be written as a linear function of j. This function can then be inverted to obtain a first guess of j from a surface current observation.
Another approach is to eliminate j from the model (8) first, and then to construct a model which has $\bar{u}$, the depth-averaged current vector, as an input instead. A first guess for $\bar{u}$ is available: one can simply use the HF radar surface current data. Under certain assumptions, elimination of j from the model is possible. One of these assumptions is that the bottom stress τ_b can be expressed as a function of depth-averaged current as

$$\tau_b = \rho_w g n^2 h^{-1/3} |\bar{u}| \bar{u} \tag{9}$$

with n the Manning coefficient. Let

$$w \triangleq u - \bar{u} \tag{10}$$

be the residual current profile. By taking the depth average of (8) and subtracting it from (8), w is shown to satisfy the following equation:

$$\dot{w} + i\gamma w - Lw = (\rho h)^{-1}(\tau_b - \tau_s) \tag{11}$$

with the same boundary conditions as u, given in (8c). Since τ_b and τ_s are now known, the system (11) can be readily solved. The solution method employed in this study is described in appendix a1. It is based on the assumption that the depth-averaged eddy viscosity varies in time but that the shape of the eddy viscosity is time-invariant, and that the depth-averaged eddy viscosity $\bar{\nu}$ can be computed from τ_b, τ_s and h according to the expression

$$\bar{\nu} = 0.0025\, d_b |\bar{u}| + 0.0167\, d_s |\tau_s/\rho_w|^{1/2} \tag{12a}$$

in which d_s and d_b equal depth h if the depth is sufficiently small such that the turbulence generated at the surface and at the bottom has spread over the entire water column; otherwise they are given by

$$d_i = 0.3\gamma^{-1}(|\tau_i|\rho_w)^{1/2} \tag{12b}$$

see the discussion in Ruijter(1988), his section 4.5. In this study, the eddy viscosity has been assumed uniform. However, other shapes are possible too.

The simplicity of the resulting model makes it a useful tool for a first assessment of the problem of reconstruction of current profiles from surface current data. Alternative sets of assumptions can be employed too to construct models driven by depth-averaged current. For example, instead of

(9), a linear relationship between the vertical gradient of the velocity and the velocity at the bottom of the form

$$-\alpha \, \partial u/\partial\sigma\big|_1 = u\big|_1 \qquad (13)$$

can be assumed. This expression is general enough to include a zero velocity at the bottom as a special case, by putting α equal to zero. In this case, it takes a little more effort to eliminate j from equation (8), but again, under the assumption of a uniform eddy viscosity, for example given by an expression of the form

$$\bar{\nu} = \delta_1(h)\left|\tau_b/\rho_w\right|^{1/2} + \delta_2(h)\left|\tau_s/\rho_w\right|^{1/2} \qquad (14)$$

a reasonably simple model results; see appendix a2.

If a horizontal density gradient is present then it will affect the eddy viscosity profile: under stable conditions (density increasing with depth), fluctuations in the vertical component of the velocity are damped, so the eddy viscosity is smaller than in the case of a uniform density.

3. Validation of the current profile model with measured data

3.1 Description of the data

Data used for validation are OTT profile measurements made by Rijkswaterstaat during the HF radar experiment in the North Sea near Den Helder in the North-Western part of the Netherlands on November 17, 1988 between 9:00 and 17:30 (see Rijkswaterstaat(1990). The measurements were made from a ship. Simultaneously, water depth and wind were measured.
The location of the measurements discussed in this report is indicated by S7 in figure 18, taken from Rijkswaterstaat(1990). The data are presented in a number of figures, for example fig. 1 (together with some model results).

Water depths measured from the ship show a very large variation in time, much larger than what should be the tidal amplitude at this location. There are two possible explanations for this. Firstly, the position of the ship changed over a distance of about 50 m due to the tidal current. Secondly, the apparent depth as measured from the ship depends on the current and is therefore in general not considered reliable.

Apparently, at the beginning velocities are high and there is little variation of the current over the depth, indicating a high value of the eddy viscosity. Later, around the turn of the tide, velocities drop and the shape of the profile becomes more fluctuating. When the velocity increases again, there is a wide variation in current over the depth, indicating that the eddy viscosity is not yet adjusted to the increased depth-averaged velocities.

3.2 Comparison of model and data

The model (11) requires as inputs depth-averaged current, wind and water level. All three could be derived directly from the measurements (depth averaged current by averaging the OTT current profile data). Several runs of the model with different sets of parameters were made, and compared with the OTT data. In addition, model inputs such as depth-averaged current, wind, and in addition, eddy viscosity were optimized to identify the causes of the observed differences between model and OTT data. For that purpose, the profile reconstruction algorithm could be employed, described in the next chapter.

In figure 1, results of a run are shown with a Manning coefficient of 0.027 (a first guess). In the first hours, with high current velocities, the measured profiles are reproduced quite well by the model. Later, near the turn of the tide when the velocities become very small, the measurements show considerable fluctuation of the current with depth, but the computed profile is almost straight. When the current picks up again, the computed profiles are still stiffer than the measured profiles. One reason for this may be an error in the depth data. Another reason can be that it takes some time for the eddy viscosity to adjust to the increased velocity. This can be expected: after a

change in the bottom stress due to the increase of the current velocity, it takes some time before the turbulent kinetic energy has adjusted to the new boundary conditions due to dissipation. This effect has not been taken into account in the present formulation (12) for the depth-averaged eddy viscosity, which assumes that the eddy viscosity responds instantaneously to the surface stress and the depth-averaged current.

The model simulations can indeed be improved somewhat by simultaneously correcting depth-averaged current and eddy viscosity, both as functions of time. The results are shown in fig. 2. The corrected eddy viscosities indicate a delay relative to the eddy viscosities from formula (12) when the velocities are increasing. However, the observed profiles around the turn of the tide cannot be reproduced at all by the model.

Still the expression for the depth-averaged eddy viscosity is somewhat better than a constant eddy viscosity: results with a constant value of 0.015 are shown in fig. 3. As an average, this value is not bad, but clearly it is too low at the beginning, and too high at the end.

To show the sensitivity to the Manning coefficient, runs were made with different values. Results with a value of 0.030 are shown in fig. 4. The value of 0.027 seems not a bad choice.

To get an idea of the sensitivity of the model to wind, a run with zero wind speed was made, see fig. 5. Wind with speeds below 12 ms^{-1} at a height of 1 to 2 do not seem to affect the current profile very much. In fact, some experiments were done with correction of the wind to optimize the fit of computed profiles to the OTT data, but the reconstructed winds were completely different from the measured winds both in magnitude and direction. Apparently, these very large wind corrections are needed to fit features of the current profile shape near the surface that are poorly represented by the model. This indicates that it may not be a good idea to correct the wind in the profile reconstruction algorithm, or at least that the magnitudes of wind corrections should be penalized.

To show the sensitivity of the model to depth, runs with a constant depth were made. Results with a depth of 10 meter are shown in fig. 6. The results are not bad, considering the large error in depth. With a constant depth of 12 m (not shown), results are somewhat worse. In practice, it is always possible to make a much better first guess of depth than just a single constant value. A first guess of depth can be derived for example from the astronomical tide or from real-time surge predictions.

Finally, fig. 7 shows a run with the same parameters as fig. 1, but without including the transients in the computation, so the computed profile is the asymptotic profile for the current boundary conditions. The results indicate little difference with fig. 1, which implies that transients are not important in this case. This is as expected: with a depth of less than 12 m and an average eddy viscosity of about 0.015, the time constant (time for a disturbance to reduce to e^{-1} times its original value) for the slowest mode (see appendix a1) is about 15 minutes. Clearly, this situation can be quite

different in a sea with a depth of say 40 m; with the same eddy viscosity, the time constant is about 2.5 hours in that case.

Concluding, the model seems to perform quite well except around and after the turn of the tide, when the variation of the current over depth is largest. Improvement can be realized in two ways.

The first is to keep the model as it is with a uniform eddy viscosity, but to improve the expression for bottom friction by using (13) instead of (9). Then bottom friction depends on eddy viscosity by (8c), and on the other hand, eddy viscosity depends on bottom friction by (14). This can be combined with a simple model of the delay of depth-averaged eddy viscosity, which is a crude description of the depth-averaged input versus dissipation of turbulent kinetic energy. With such a model, it will probably not be possible to model the profile accurately when the depth-averaged velocity is very low. However, in the situation of increasing depth-averaged velocity following the turn of the tide, the situation may improve.

The second option is to use a discretized version of the model (8), with a k-ε model to compute the eddy viscosity, and with a nonlinear boundary condition at the bottom. In that case, j (see chapter 2) has to be corrected instead of the depth-averaged current, but this will not be a problem. This is still a 1DV model so it does not require to much computation. However, the effort required for a numerically robust and accurate implementation is expected to be considerable. It may be simplified by modeling the momentum balance as steady (which is a fair approximation) and including dynamics only in the solution of the kinetic energy balance, but in any case, it will require more effort than the simple models as employed in this study.
An advantage of this approach is that it shows the essential potential and limitations of the profile reconstruction method. Moreover, it offers the possibility to deal with stratification in a rigorous way.

4. The reconstruction algorithm

4.1 Basic concepts

The reconstruction of the model inputs (depth-averaged velocity, wind, water level) is based on a straightforward statistical criterion. In this case, it takes the form of minimizing the sum of squared differences between the computed surface current vector and the observed surface current vector, that is,

$$\hat{\theta} = \underset{\theta \in A}{\arg\min} \sum_{i=1}^{n} \| u_i^o - g_i(\theta) \|^2 \qquad (15)$$

in which
θ is the sequence of model inputs to be reconstructed, taking its values in a space A, and
$g_i(\theta)$ is the computed surface current at the instant labelled i, at which a surface current observation u_i^o is available. So $g_i(\theta)$ is determined by the numerical model.
n is the number of observations used to reconstruct θ.

The current profile at the current instant is a function of the inputs θ, so once $\hat{\theta}$ has been reconstructed, it can be computed by running the model.

This criterion corresponds to the assumption that the observation errors are independent gaussian random vectors with zero mean and equal variance, and that the components of each of these vectors are independent and identically distributed too (e.g. De Valk, 1990). Whether this is a valid assumption is not known, but at least this criterion will do for the moment. As a remark, for the case of OTT current measurements, this criterion does certainly not apply; in that case it would be better to assume errors in observations of magnitude and velocity to be independent instead.

If first guesses of the model inputs are available that provide some information in addition to the information from the measurements, a term should be added in the criterion to penalize the deviation of θ from its first guess. In this study, this has not been done, since the primary goal is to test the principles. In a final implementation, such a term may be included though.

4.2 Observability of the current profile model

Observability pertains to the question whether the state (current profile) can be reconstructed from the observations (surface current), given the fact that the inputs (depth-averaged velocity or "slope" j, and possibly wind and water level) are not known. This subject requires a discussion of what kind of observability requirement applies here exactly, which is certainly not trivial. However, if the dynamics of the current profile is neglected, it is not complicated at all. This approach makes sense, because if the state is not observable when the dynamics are neglected, then in practice reconstruction of the state will not work well, even if formally (including the dynamics) it would be observable (in the proper sense).

The solution of (8a) obtained when the term $\dot{u}$ is neglected is of the form

$$u = \beta_1 j + \beta_2 \tau_s \qquad (16)$$

with β_1 and β_2 functions that depend on the eddy viscosity and the depth h, so the surface current is given by $u(0) = \beta_1(0) j + \beta_2(0)\tau_s$.

Assume first that h is known, and that eddy viscosity depends again on the current profile u, so it is not required as a model input. Clearly j and τ_s cannot both be reconstructed from a surface current observation. Therefore, we must assume that one of them is known, or we must apply a statistical criterion to the reconstruction which involves prior knowledge of j and/or τ_s, so a statistically optimal reconstruction can always be computed. This does not mean that such a reconstruction will be of any value; it can be optimal, but very poor if the prior knowledge is insufficient. A similar conclusion follows if for example j is eliminated from the model, and the depth-averaged current $\bar{u}$ appears.

In practice, this conclusion does not have serious consequences. A fair guess of the wind vector can always be made, and the sensitivity of the profile to the wind is rather small, at least in the case studied in chapter 3. In such a situation, the bottom stress appears to be about an order of magnitude larger than the wind stress, so inaccurate wind data may be good enough. Available water level data are generally also good enough, because the model is not very sensitive to water level either. So if the only unknown is j (or depth-averaged velocity), the problem is solvable. Including dynamics in the approximate momentum balance (8) will not change this conclusion in practice, since the effect of the dynamics will be small. If the eddy viscosity is made to satisfy a dynamic model, the conclusion also does not change since it still depends completely on the state u in such a manner that it is unlikely to have any effect on observability.

4.3 Description of the reconstruction algorithm

Recall from 4.1 that in order to reconstruct the model inputs θ, a function should be minimized that we call here f, which is of the form

$$f = \sum_{i=1}^{n} \| u_i^o - g_i(\theta) \|^2 \qquad (17)$$

Minimizing f requires running the model to compute $g_1(\theta),..,g_n(\theta)$ for different values of the model inputs θ, and computing the gradient of f with respect to θ. This gradient is computed by the adjoint model which is derived from the well-known chain rule of differentiation (see for example the appendix of De Valk and Calkoen, 1989).
For the minimization, a descent method (conjugate gradient method, of BFGS for example, in this case a limited-memory version of BFGS described in De Valk and Calkoen(1989) can be used, based on the full-memory BFGS implementation of Dennis and Schnabel(1983). This algorithm calls routines to evaluate f and its gradient, and stops when stopping rules indicate that the estimate is sufficiently close to a minimum.
The model inputs are time sequences of, for example, depth-averaged current (or also wind, water level). These are not adjusted independently at every model time step, since the scale of the temporal variation of these inputs should be determined independently from the numerical model itself. Therefore, the perturbation of the first guess of a model input has been represented as a B-spline, that is, as a linear combination of B-spline basis functions (De Boor, 1983). This basis is a local one. In this study, cubic splines were used. For the purpose of obtaining the contribution of a particular spline coefficient to the value of the spline at a certain instant, a very compact routine was used.

The complete algorithm was implemented on PC. The computations for different spatial locations can be carried out simultaneously. A special data structure for storage of observations was applied, which makes it possible to add new types of observations, if required, by simply linking extra subroutines. Disk caching was used to attain a high speed without having to reduce the IO for storage of data that have to be passed from the model to its adjoint.
Alternative implementations of the model and the reconstruction method are possible. For example, the dynamics can be neglected completely which simplifies the adjoint considerably, since it does not have to be integrated backward in time. However, in this study, the most general approach was adopted. This made it easier to explore all possibilities, to deal with surprises and to have a product available that can be applied to a wider range of conditions than those encountered in the tests described in chapter 5 of this report. For example, it appears that the eddy viscosity shows some kind of dynamic behavior (see chapter 3) which can now easily be incorporated. In fact, the system that has been developed cannot only be used for processing of surface current data but for any kind of current data. It may also be valuable as a research tool.

5. Test of the profile reconstruction method with measured data

5.1 Description of the data

The data used in the tests were collected in the experiment off the coast of the North of Holland (Rijkswaterstaat, 1990) at the location S7 (see figure 18) in November of 1988. A description of the experiment and the data can be found in Rijkswaterstaat(1990). In this chapter, N will indicate North, W West, etc.

The HF radar surface current data were collected at intervals of approximately half an hour at all locations. At some instants, no data are available however. Because a single time-index was assigned to all data resulting from a scan of the area, the uncertainty in the exact time of a measurement ranges up to about half an hour. In view of the rather rapid changes that occur in the current profile (see also chapter 3), this uncertainty should not be more than about ten minutes. Therefore, it is recommended to include the exact time of the measurement with the data of each location.

As reference data, the OTT current measurements described in section 3.1 were used, as well as NBA data, both at the same location S7. The NBA current measurements were made at constant heights of 3.55 m and 7.30 m above the sea bottom.

In fig. 8, OTT, NBA and HF radar data are plotted for November 17, 1988 between 9:00 and 17:30 (together with the current profiles derived from the HF radar data). HF radar data were interpolated to the instants at which OTT and NBA data were available. Some clear inconsistencies appear.

During the first hours, the N component of the NBA current data is larger than the N component of the OTT data. It is not clear which instrument gives more reliable values. Later however, OTT and NBA data become more consistent.

HF radar data (plotted here at the surface, although they may apply to a surface layer) are quite consistent with the OTT data at the beginning. About the turn of the tide, some deviations appear: the strong fluctuations in the OTT profile are not apparent in the HF data. A large deviation of OTT current direction from HF current direction occurs from 15:00 to 16:00. Inspection of the hand-written OTT data learned that problems with calibration of the instrument occurred around this time, so probably the OTT directions are not reliable here. This holds also for 17:30, were it has been mentioned that no calibration could be performed due to high wind sea.

In figs. 10 and 11, HF radar data and NBA data at 7.50 m above the bottom have been plotted as functions of time over the period November 14, 1982, 18:00 to November 18, 1991, 23:30.

Except at the very end of this period, the directions of the HF radar data

contain very large fluctuations, in particular when the NBA current direction is SSW. This has not been mentioned in Rijkswaterstaat (1990); in fact, it does not discuss the measurements of current directions in the North of Holland at all. HF radar measurements of current direction in Zeeland, obtained from the same instrument, show generally very good agreement with measurements by other instruments. Therefore, the error in the HF radar current directions shown in figs. 10 and 11 is probably due to system failure or to a problem with the system that appears only under certain conditions.

Apart from these fluctuations, there is also a systematic difference between the directions measured by HF radar and by NBA; see figs. 10 and 11. The N component of the HF radar current vector (indicated u in fig. 10) has a smaller magnitude, and the W component a larger magnitude than found in the NBA data.
In fact, it seems that the HF radar direction is biassed towards the beam directions; the observed fluctuations in the HF radar current direction are also between the NBA current direction and one of the beam directions. This indicates that the observed differences are due to an error in the HF radar data. On the other hand, the comparison of NBA and OTT data (see above) showed that the N component of the NBA current vectors was larger than the N component of the OTT current vectors during the first hours of the OTT measurement at November 17, and HF radar and OTT data were more consistent than NBA and OTT data during that period, which points to an error in the NBA data or to a systematic difference due to the distance between the sensors. So there is no reason to assume that the HF radar data are wrong.
The magnitudes of HF radar and NBA current vectors agrees quite well in general, maybe even too well, given the fact that the NBA data were collected at several meters below the surface.

One reason for the differences between OTT, NBA and HF radar data may be the differences in location. In particular, due to the movements of the ship, the OTT data are not all at exactly the same location. It is very likely that some deviations of the HF radar data from OTT or NBA data are caused by the circumstance that the exact time of the HF radar measurements is not known.

For the first test described in 5.2, wind and water depth data needed as input data in the model were interpolated from the measurements made from a ship during the OTT current profile measurement.

For the first test described in 5.3, water level data were derived from measurements in Julianadorp, a location at the coast at about 5 km south of S7. Wind data were taken from measurements at Den Helder, since they were considered more reliable than the measurements on top of a dune in Julianadorp.

5.2 Short test with HF radar measurements: comparison with OTT and NBA data

The profile reconstruction was tested with HF radar data collected at the location S7 at November 17, 1988 between 9:00 and 17:30. In the tests, current profiles were reconstructed from the HF radar surface current measurements only. Data from the OTT and NBA were merely used to evaluate the profile reconstructions.
In the first run, wind and depth were taken directly from the measurements. The first guess for depth-averaged current was taken equal to the HF radar surface current data. Then the algorithm was used to reconstruct the depth-averaged current. The resulting current profile estimates are shown in fig.8 together with the HF radar data (if available) and the OTT and NBA data for comparison.
In all cases, the reconstructed profiles fit the HF radar data exactly; this is because the number of spline coefficients used to represent the depth averaged current velocity was large enough to produce an exact fit.
In general, the fit with the OTT and NBA data is quite good, considering the order of magnitude of differences between data of different sensors. Around the turn of the tide, the reconstructed profiles are stiffer than the OTT profiles (see also chapter 3). A very large deviation is found from the OTT data at 15:00-16:00, but the fit with NBA data is good. In view of the problems with the calibration of the OTT mentioned in 5.1, it is probably not fair to ascribe these difference to reconstruction errors. The fit to NBA data is almost always good except at the beginning.
Some deviations can possibly be ascribed to differences in location of the measurements by different instruments. The difference between reconstructed profiles and either OTT or NBA data seems not larger than the difference between OTT and NBA.

Since the model is little sensitive to wind, errors in the wind input will have little effect on the reconstructions (see section 3.2). To show the effect of errors in the depth (again correcting only the depth-average current), a test run was made with depth equal to 10 m; see fig. 9. Taking the depth constant leads to some extra error, which, however, is not very serious. A constant depth of 10 m is really a very poor first guess; in practice, one can always do much better than that.

5.3 Long test with HF radar measurements: comparison with NBA data

Another test of the profile reconstruction method was carried out with HF radar data collected at the location S7 over the period November 14, 1988 18:00 to November 18, 1988 24:00. This time interval was divided in four subintervals of approximately equal length, and the test was performed separately on each subinterval.
The HF radar data were taken as first guesses of depth-averaged current. Water depths were derived from water level data at Julianadorp, simply by subtracting the local sea bottom height from the water level at Julianadorp (both expressed in meters above NAP). No attempt was made to correct for phase or amplitude differences between Julianadorp and S7. Wind data were interpolated from the 6-hourly measurements at Den Helder.

The resulting profile reconstructions were compared with NBA current measurements at S7 at 3.55 m and 7.3 m above the sea bottom. Results are shown in figures 10 to 13.

At 7.3 m above the sea bottom (see figures 14 and 15), the reconstructed currents are very similar to the HF radar current data from which they were derived. In particular the fluctuation in the direction with SSW current direction is quite obvious. If this is neglected, then the W component of the reconstructed current vector agrees quite well with the W component of the NBA current data. Of course this was also the case for the original HF radar data. Due to the large apparent errors in the HF radar data, the slight improvement of the reconstructions compared to the crude HF radar is barely noticeble. A similar conclusion applies to the other component of the current vector, but here there is a systematic difference in amplitude just as was found in the comparison between HF radar and NBA data in section 5.1.

At 3.55 m above the sea bottom (see figures 16 and 17), the differences between the reconstructed current vector and the measured current vector are similar to those at 7.3 m above the sea bottom. Again the fluctuations in the HF radar current direction show up in the reconstruction. The W component of the reconstructed current vector is again very close to the NBA data, and the N component of the reconstructed current vector has smaller amplitude than in the NBA data. Interesting about the results at this height is that now the improvement over the crude HF radar data is quite significant, as can be seen by comparing fig. 16 with a plot of HF radar data and NBA data at 3.55 m in fig. 12. In particular the W component has improved considerably. Apparently, the N component does not improve because the amplitudes become too small in comparison with the NBA data, but it is interesting to see that the results are quite consistent with those at 7.5 m (fair agreement of W component, amplitude of N component smaller than in NBA data). In fact, by comparing figs. 12 and 10, it becomes clear that the correspondence in amplitude of the N components of HF radar current and NBA current at 3.55 m is a consequence of the fact that at 7.30 m, the amplitude of the HF radar is much smaller than of the NBA data. Therefore, the model is probably correct, but NBA data and HF radar data are not consistent (due to an error in either one of these sensors, or to a difference in location; see 5.1).

We conclude that the model and the reconstruction seem to work quite well, and the differences between reconstructions and NBA data appear mainly to be caused by errors in the HF radar data (strongly fluctuating direction) and by other inconsistencies between NBA data and HF radar data. Due to these inconsistencies, the N component of the reconstructed current vector has a smaller amplitude than in the NBA data at both levels above the sea bottom.

It is recommended to stufy in more detail the source of the errors in the measurements of current direction by HF radar, to find out whether this is an incidental failure or a limitation of the technique. If it cannot be corrected, it may be a good idea to implement an automatic data validation algorithm which removes data that are unreliable. The fluctuations in the HF radar current direction can for example be detected by an adaptive least squares predictor (Goodwin and Sin, 1984; Ljung and Soderstrom, 1983), which projects the measured signal on a basis of sinusoids corresponding to the dominant tidal components. If the prediction error exceeds a certain expected value, then the data at that instant are clearly inconsistent with the data in the past, and are either discarded or, if the nature of the error is well-known, corrected.

5.4 Conclusions

The results obtained so far indicate that, in principle, the method works. Because errors in depth seem not to matter much, depths can be fixed at their first guesses. The same holds for wind in the test situation, but due to the quadratic friction law, significant effects of wind can be expected with very high wind speeds. So possibly wind should be corrected too, but with a penalty on deviations from its first guess to ensure that wind corrections are effectuated only if wind speeds are very high. Under normal conditions, this term should be negligible. Right now, the main source of error in the reconstruction algorithm seem to be the shortcomings of the model. Suggestions for improvement have been given in section 3.2.

Comparison with NBA data shows that there are large errors in the directions of the HF radar current measurements, which affect the profile reconstructions. It is recommended to investigate the source of these errors. An automatic data validation procedure based on an adaptive predictor is proposed to detect these errors. In addition, a difference in amplitude of the N component of the reconstructed current vectors and the NBA current vectors was found, which is most likely due to inconsistency between HF radar data and NBA data. More extensive testing with data at other locations is needed in order to assess the real value of the reconstruction method, and to get a better picture of the error characteristics of HF radar current data.

6. Feasibility and potential of the method

An HF radar system installed at the coast can reach over a distance of 30-50 km. The most important region for applications is probably close to the coast, at depths of less than 15 m. Important regions for applications to transport of sediment and pollutants are near tidal inlets. The data used in the tests of the reconstruction method and the model were collected in such a region, so results of the tests with these data can be considered as representative. In deeper water, transients may become more important, but the overall behavior of the current profile will not differ much from that observed in this study.

In section 4.2, it was concluded that only reconstruction of the depth-averaged velocity is possible (or equivalently: the forcing j of the model (8)). In section 3.2, it was concluded that the model is not very sensitive to errors in the wind, so correction of the wind is not needed in practice except possibly under severe storm conditions. Available first guesses of the wind such as predictions or analyses from the weather service are probably good enough. It was also concluded that available first guesses of depth will be good enough in practice, so adjustment of depth will not be required either. Therefore, the fact that only depth-averaged velocity can be corrected will cause any problem in practice because wind and depth do not have to be corrected.

The achievable improvement over simply using the HF data depends on tidal phase and possibly on conditions like wind. A strong tidal current over several hours causes stiff profiles, so relatively little can be gained. However, it is not difficult so result can be accurate. Around and after the turn of the tide, a substantial gain is possible (large fluctuations over the profile), but the profiles are more difficult to model and to reconstruct. In the latter situation, the very simple model applied in this study is not good enough; a more realistic, and consequently more complex model is required.

The computational requirements of the method as implemented in this study are modest: execution of the computation once every half hour at the maximum number of HF radar data locations of up to 700 will be no problem. If a more complex model is used, possibly the number of locations may have to be limited, but even then, computational requirements are not expected to become an essential limitation. Probably it will be sufficient to reconstruct the current profiles at a fraction of the maximum number of locations of the HF radar data.

Operational application requires data-bases of HF radar surface current data (which are required anyway) and of profile reconstructions. It also requires facilities to display the information, either at a single point in the plane or over an area. Both off-line and real-time applications are foreseen. The volume of data that becomes available is quite large compared with most conventional measurement techniques, in particular because the current profile reconstruction produces a three-dimensional data set. Therefore, the most likely option for permanent archiving of data is to store only the surface current data, and to use the reconstruction algorithm to generate profiles

only when these are needed. In this concept, a data-base with current profile data is only for provisional storage, needed for real-time applications. A detailed analysis of possible applications and of user requirements should be carried out before starting the design.

7. Conclusions and recommendations

1. A technique for reconstruction of current profiles from surface current data has been proposed, based on a 1DV model of the current profile evolution. Results of tests demonstrate that in principle, the method works.

2. The method realizes the profile reconstruction by adjusting the inputs of the 1DV model. It appears that adjustment of depth-averaged current (or equivalently, of a forcing term containing the surface slope) is most important. The effects of wind and water level are small, so available first guesses are in general good enough, and wind correction may be needed only under storm conditions.

3. Comparison of the profile reconstructions with NBA current measurements at two different heights above the sea bottom indicates that the main source of error in the reconstructions is a fluctuation in the HF radar current direction. Apart from this, there appears to be a systematic difference in the amplitude of the N component of the reconstructed current vector and of the NBA current vector. This may be due to an abberation in one of the instruments, or to a difference in location. More extensive testing and comparison with other data is required to resolve these matters. In section 5.3, an automatic procedure for validation of current data is proposed to detect errors in HF radar data.

4. A detailed comparison of the profile reconstructions with OTT current profile measurement shows that the achievable improvement compared to crude surface current measurements depends on tidal phase. The limitations of the 1DV model are most clearly visible when the achievable improvement is most significant. This implies that the profile reconstructions can be improved by improving the 1DV model.
Observed differences between 1DV model output and OTT current profile data are the profile shapes around and after the turn of the tide.

5. Improvement of the model can be approached in two ways:

A simple approach is to improve the boundary condition at the bottom, to change the shape of the eddy viscosity profile, and to solve a depth-averaged kinetic energy balance to model the dynamics of the eddy viscosity. In addition, an effort should be made to make a version of the model that is also suitable in situations with profound stratification.

A more fundamental approach is to use a 1DV k-ε model (possibly with some simplifications). Only the latter approach can identify the full potential and the essential limitations of the reconstruction method. In particular, stratification can be dealt with in a rigorous manner. However, the effort required to carry out this program is much larger than for the simple approach. Since it is far from certain that this effort will pay off, the simple approach is recommended.

6. It is recommended to study possible model improvements first, and then to perform more comprehensive tests with other available data sets.

7. The profile reconstruction method requires little computation, so routine operation seems quite feasible, even if a more complex 1DV model is used.

8. Recommendations pertaining to operational application are given in chapter 6. It is recommended to store the original surface current, wind and water level data required for profile reconstruction; the profile reconstruction can be carried out when the profile data are needed.

9. For the purpose of current profile reconstruction, it is recommended to archive the exact time of an HF radar surface current observation for each separate location.

REFERENCES

Chavent, G.(1980): Identification of distributed parameter systems - about the output least squares method, its implementation, and identifiability. Proc. 5th IFAC symposium on identification and system parameter estimation, vol.1. Pergamon Press, New York, pp 85-97.

Davies, A.M.(1987): On extracting current profiles from vertically integrated numerical models. Coastal Engineering vol.11, pp 445-477.

Davies, A.M.(1988): On formulating two-dimensional vertically integrated hydrodynamic numerical models with an enhanced representation of bed stress. Journal of Geophysical Research, vol.93, no.C2, pp 1241-1263.

De Boor, C.(1985): A practical guide to splines. Springer Verlag, New York.

Dennis, J.E. and R.B. Schnabel(1983): Numerical methods for unconstrained optimization and nonlinear equations. Prentice-Hall Inc., New Jersey.

De Valk, C.F. and C.J. Calkoen(1989): Wave data assimilation in a 3rd generation wave prediction model for the North Sea - an optimal control approach. DELFT HYDRAULICS report X38, Delft.

De Valk, C.F.(1990): Assimilation of TIR imagery into numerical models as a tool for water management. DELFT HYDRAULICS report H971, Delft.

Goodwin, C.G. and K.S. Sin (1984): Adaptive filtering, prediction and control. Prentice-Hall, Englewood Cliffs, N.J.

Ljung, L. and T. Soderstrom (1983): Theory and practice of recursive identification. MIT Press, Cambridge, Mass.

Luenberger, D.G.(1969): Optimization by vector space methods. Wiley, New York.

Rijkswaterstaat(1990): Toetsing van de bruikbaarheid van het HF radar systeem voor het meten van oppervlaktestromingen middels metingen in Zeeland en Noord-Holland in november 1988. Draft Report (in Dutch).

Ruijter, M.N.(1989): Voorspelling can de oppervlaktestroming - ondersteuning van de Nederlands zeilploeg tijdens de olympische spelen in september 1988 (MSc thesis). DELFT HYDRAULICS report H811, Delft.

Sage, A.P. and J.L. Melsa(1971): System identification. Academic Press, New York.

Zitman, T.J.(1991): Quasi 3-dimensional current modelling by applying a modified version of Davies' shape function approach. To appear in: Continental Shelf Research.

APPENDIX

a1. A simplified method for the solution of the momentum balance

a1.1 Basic solution method

This appendix describes a method for the solution of equation (11) for the residual current profile, that is

$$\dot{w} + i\gamma w - Lw + (\rho_w h)^{-1}(\tau_s - \tau_b) = 0 \qquad (20a)$$

Assume that the viscosity is the product of its depth average N with a time-independent shape function ϕ, as

$$\nu = N\phi \qquad (20b)$$

Then the differential operator L (see (8b)) becomes

$$L \triangleq h^{-2} N\, \partial/\sigma\ \phi\partial/\partial\sigma \qquad (20b)$$

and the boundary conditions for (20a) are

$$-\rho_w h^{-1} N\phi\ \partial w/\partial\sigma\big|_0 = \tau_s \qquad -\rho_w h^{-1} N\phi\ \partial w/\partial\sigma\big|_1 = \tau_b \qquad (20c)$$

Consider first the steady solutions of (20), i.e. solutions of

$$i\gamma w - Lw + (\rho_w h)^{-1}(\tau_s - \tau_b) = 0 \qquad (21)$$

with the boundary conditions (20c). These solutions can be written as

$$\tau_s f_s - \tau_b f_b \qquad (22a)$$

with f_s and f_b functions satisfying

$$< 1, f_i > = 0 \qquad i = s,b \qquad (22b)$$

$$i\gamma f_i - Lf_i + (\rho_w h)^{-1} = 0 \qquad i = s,b \tag{22c}$$

and the boundary conditions

$$\begin{aligned} -\rho_w h^{-1} N\, \phi \partial f_s/\partial\sigma\big|_0 &= 1 \quad -\rho_w h^{-1} N\, \phi \partial f_s/\partial\sigma\big|_1 = 0 \\ -\rho_w h^{-1} N\, \phi \partial f_b/\partial\sigma\big|_0 &= 0 \quad -\rho_w h^{-1} N\, \phi \partial f_b/\partial\sigma\big|_1 = -1 \end{aligned} \tag{22d}$$

Now we are ready to solve (20). Define at each instant of time:

$$\tilde{w} = w - \tau_s f_s + \tau_b f_b \tag{23}$$

i.e. $\tilde{w}$ is the difference between the current residual profile and the steady residual profile corresponding to the instantaneous values of τ_s and τ_b. Now (20) can be written as

$$\dot{\tilde{w}} + i\gamma\tilde{w} - L\tilde{w} + d/dt\,[f_s\tau_s - f_b\tau_b] = 0 \tag{24a}$$

with

$$d\tilde{w}/d\sigma\big|_0 = 0 \qquad d\tilde{w}/d\sigma\big|_1 = 0 \tag{24b}$$

and f_s and f_b given by (22). This version is much more useful than (20), because the boundary conditions are now independent of τ_s and τ_b.

Consider $\tilde{w}$ as an element of $\mathcal{L}_2[0,1]$, the space of functions on [0,1] for which the inner product

$$< f,g > = \int_{[0,1]} f(\sigma)^* g(\sigma)\, d\sigma \tag{25}$$

is defined, and the norm $\|f\|_2 = < f,f >^{1/2} < \infty$. Note that in $\mathcal{L}_2[0,1]$, two functions f and g are identical when $\|f-g\|_2 = 0$.

Let $\mathcal{D}$ be the linear subspace of $\mathcal{L}_2[0,1]$ consisting of all elements of $\mathcal{L}_2[0,1]$ that satisfy the boundary conditions (15b). The operator L in (15a) (see (10b)) is self-adjoint in $\mathcal{D}$, which means that $\mathcal{D}$ is spanned by an orthonormal basis of eigenfunctions of L, i.e. functions $\{g_1, g_2, \ldots\}$ satisfying

$$Lg_k = \varepsilon_k g_k \quad \text{in } (0,1) \qquad k= 1,2,... \tag{26a}$$

$$\|g_k\| = 1 \qquad k= 1,2,... \tag{26b}$$

$$dg_k/d\sigma\big|_0 = 0 \qquad dg_k/d\sigma\big|_1 = 0 \qquad k= 1,2,... \tag{26c}$$

Define

$$a_k \triangleq < g_k, \tilde{w} > \qquad k= 1,2,... \tag{27}$$

Because $\tilde{w}\epsilon\mathcal{D}$, and the functions g_k, k=1,2,.. are orthonormal and span $\mathcal{D}$,

$$\tilde{w} = \sum_{k=1,2,..} a_k g_k \tag{28}$$

The dynamics of the coefficient a_k is given by taking the inner product of g_k with the left hand side of (24a):

$$\dot{a}_k + i\gamma a_k - < g_k, L\tilde{w} > = - d/dt \; [\; <g_k,f_s>\tau_s - < g_k,f_b >\tau_b \;] \tag{29}$$

k=1,2,3,....

Because g_k and $\tilde{w}$ are in $\mathcal{D}$,

$$< g_k, \; L\tilde{w} > = < Lg_k, \; \tilde{w} > \tag{30}$$

so (29) becomes, with (26)

$$\dot{a}_k + (i\gamma - \varepsilon_k)a_k = - d/dt \; [\; < g_k,f_s >\tau_s - < g_k,f_b >\tau_b \;] \tag{31a}$$

k=1,2,3,...

The residual profile w can now be computed by

$$w = \sum_{k=1,2,..} a_k g_k + f_s\tau_s - f_b\tau_b \tag{31b}$$

Observe that this system satisfies the boundary conditions *exactly* at each instant. Moreover, the approximation of (28) by a finite series can lead to

inaccuracies only when τ_b and τ_s vary in time. For steady τ_b and τ_s, the solution is exact.
An advantage of (31) is that the quasi-steady component and the transient component of w are computed separately, which makes it possible to compare them, and to simplify the model to a quasi-steady model if desired.

In the next section, (31) will be worked out analytically for the case of a uniform eddy viscosity. Nunerical approximation of the basis $\{g_k,\ k=1,2,..\}$ is possible in principle for other kind of eddy viscosity profile shapes, by solving the corresponding eigenvalue problem.

a1.2 solution for the case of a uniform eddy viscosity profile.

In the case of a uniform eddy viscosity, ϕ equals unity in [0,1] and we have

$$g_k(\sigma) \triangleq 2^{1/2}\cos(\pi k\sigma) \qquad \sigma\in[0,1] \tag{32}$$

k=1, 2, 3, ...

so

$$\varepsilon_k = -\pi^2 k^2 N/h^2 \tag{33}$$

In this case, (22) is satisfied by functions f_i of the form

$$f_i = d_{1,i}\exp(z\sigma) + d_{2,i}\exp(-z\sigma) - (i\gamma\rho_w h)^{-1} \qquad i = s,b \tag{34a}$$

with

$$z \triangleq (i\gamma/N)^{1/2}h \tag{34b}$$

The coefficients $d_{1,i}$ and $d_{2,i}$ in (34a) must be chosen to satisfy the boundary conditions (22d). This leads to the general solution

$$f_s = (\beta z[\exp(z(1-\sigma)) + \exp(-z(1-\sigma))] - 1)/\rho_w hi\gamma \tag{35b}$$

$$f_b = (\beta z[\exp(z\sigma) + \exp(-z\sigma)] - 1)/\rho_w hi\gamma \tag{35c}$$

with

$$\beta \triangleq [\ (\exp(z)-\exp(-z))\ ]^{-1} \qquad (35c)$$

Moreover, in (31a)

$$< g_k, f_s > = 2^{1/2}(\pi^2 k^2 z^{-2} + 1)^{-1}/\rho_w hi\gamma \qquad (36a)$$

$$< g_k, f_b > = (-1)^k < g_k, f_s > \qquad (36b)$$

a1.3 discretization

For an arbitrary eddy viscosity profile, (31a) is discretized as follows. Interpolate ε_k and $< g_k, f_s >_{\tau_s} - < g_k, f_b >_{\tau_b}$ linearly between two instants at which they are known, labelled i-1 and i. The exact solution of (31a) with this forcing (the so called "equivalent discrete model" of (31a)) is then:

$$a_k^i = \alpha_{1,k}^i a_k^{i-1} + \alpha_{2,k}^i (F_k^i - F_k^{i-1}) \qquad (37a)$$

with

$$\alpha_{1,k}^i \triangleq \exp(\lambda_k^i \Delta t) \qquad (37b)$$

$$\alpha_{2,k}^i \triangleq [1 - \exp(\lambda_k^i \Delta t)]/\lambda_k^i \Delta t \qquad (37c)$$

Δt the time step,

$$\lambda_k^i = (\varepsilon_k^i + \varepsilon_k^{i-1})/2 - i\gamma \qquad (37d)$$

$$F_k^i = < g_k, f_s^i >_{\tau_s^i} - < g_k, f_b^i >_{\tau_b^i} \qquad (37e)$$

The residual profile w can now be computed by

$$w^i = \sum_{k=1,2,..} a_k^i g_k + f_s^i \tau_s^i - f_b^i \tau_b^i \qquad (38)$$

For the case of a uniform eddy viscosity over [0,1],

$$\varepsilon_k = -\pi^2 k^2 N/h^2 = -\pi^2 k^2 z^{-2} i\gamma \qquad (29)$$

so

$$\lambda_k^i = -i\gamma \left[\pi^2 k^2 ((z^i)^{-2} + (z^{i+1})^{-2})/2 + 1\right] \qquad (30d)$$

and

$$F_k^i = 2^{1/2} (\pi^2 k^2 (z^i)^{-2} + 1)^{-1} (\rho_w hi\gamma)^{-1} (\tau_s^i - (-1)^k \tau_b^i)$$

$$z^i = (i\gamma/N^i)^{1/2} h^i \qquad (30h)$$

a2. An alternative method for the solution of the momentum balance

In this approach, we start from equation (8) for the current profile itself, that is

$$\dot{u} + i\gamma u + j - Lu = 0 \qquad (31a)$$

L is again assumed of the form (20b), (20c).
The difference with the approach of appendix a1 is that we do not consider the bottom stress to depend on the depth-averaged current, but (more correctly) the bottom stress τ_b depends on the flow near the bottom, so it cannot be considered as an external forcing term.
In order to solve (31a), we will assume a simple linear time-invariant relationship between the vertical gradient of the velocity and the velocity at the bottom of the form

$$-\alpha \partial u_i / \partial \sigma \Big|_d = u \Big|_d \qquad i=1,2 \qquad (31b)$$

This expression for bottom stress is general enough to include a zero velocity at the bottom as a special case, by putting α equal to zero. Assumption (31b) is equivalent to the assumption that the bottom stress is of the form

$$\alpha \tau_{b,i} / \rho_w = N \phi h^{-1} u \Big|_d \qquad i=1,2 \qquad (32)$$

The proportional dependance of bottom stress on h^{-1} is not convincing if the eddy viscosity is kept fixed, but it may be a reasonable assumption if N is linear in h, which is indeed the case in certain empirical expressions for N (for example (14) with δ_1 and δ_2 proportional to h). In that case, the factor relating bottom stress to velocity at the bottom is essentially independent of depth. The boundary condition at the surface is again

$$-h^{-1} N \phi \partial u / \partial \sigma \Big|_0 = \tau_s / \rho_w \qquad (31c)$$

The model of the current profile dynamics with these boundary conditions has been proposed by Zitman(1990).

The term j in (31a) contains in the first place the surface slope. The surface slope is not known in current profile reconstruction; even making a first guess for the slope will not be easy. Moreover, in addition to the slope, j contains depth averages of the terms in the shallow-water equations involving horizontal gradients. In quasi 3D modeling, the complete j and not just the slope should be inserted in the model (31a) of the vertical structure, in order to be consistent with the 2DH computation.
In this appendix, a model driven by j is derived, based on ideas from

Zitman(1990). Then it will be shown that this model can be converted to a slightly more complex model driven by depth-averaged velocity instead. This latter model is quite useful for postprocessing of 2DH flow simulations, for quasi-3D flow simulation and for reconstruction of current profiles from an incomplete set of observations.

Equation (31) has an inhomogeneous boundary condition, (31c). Therefore, to solve (31), the first action to be taken is to rewrite it in such a way that the boundary conditions become homogeneous. This can be achieved by subtracting from u a known function of τ_s which statisfies the boundary conditions (31c). One such function is the steady profile corresponding to the instantaneous boundary conditions, i.e. the solution $\tilde{u}$ of (see (31a)

$$i\gamma\tilde{u} - L\tilde{u} = -j \tag{33a}$$

with boundary conditions, from (31),

$$-h^{-1}N\,\phi\partial\tilde{u}/\partial\sigma\big|_0 = \tau_s/\rho_w \qquad -\alpha\,\partial\tilde{u}/\partial\sigma\big|_1 = \tilde{u}\big|_1 \tag{33b}$$

The solution $\tilde{u}$ of (33) is a linear function of the surface stress τ_s and j:

$$\tilde{u} = \beta_1 j + \beta_2 \tau_s \tag{34}$$

for some functions β_1 and β_2 on (0,1), which depend on N and h. Define

$$v = u - \tilde{u} \tag{35}$$

i.e. v is the difference between the current profile and the steady profile corresponding to the instantaneous values of τ_s and j. Now from (31) and (33)

$$\dot{v} + i\gamma v - Lv = -\dot{\tilde{u}} \tag{36a}$$

with

$$dv/d\sigma\big|_0 = 0 \qquad -\alpha\,dv/d\sigma\big|_1 = v\big|_1 \tag{36b}$$

This version is much more useful than (31),because the boundary conditions are now independent of τ_s and τ_b.

From now, the approach is similar to the one shown in appendix a1. Consider v as an element of the subspace $\mathcal{D}^1$ of $\mathcal{L}^2(0,1)$ consisting of all square integrable functions that have a square integrable second derivative, and which satisfy the boundary conditions (36b). $\mathcal{D}^1$ is spanned by an orthonormal

basis of eigenfunctions of L, i.e. functions $\{g_1, g_2, \ldots\}$ satisfying

$$Lg_k = \varepsilon_k g_k \quad \text{in } (0,1) \qquad k = 1,2,\ldots \tag{37a}$$

$$\|g_k\| = 1 \qquad k = 1,2,\ldots \tag{37b}$$

$$dg_k/d\sigma\big|_0 = 0 \qquad -\alpha\, dg_k/d\sigma\big|_1 = g_k\big|_1 \qquad k = 1,2,\ldots \tag{37c}$$

Define

$$a_k \triangleq \langle g_k, v \rangle \qquad k = 1,2,\ldots \tag{38}$$

Because $v \in \mathcal{D}$, and the functions g_k, $k=1,2,..$ are orthonormal and span $\mathcal{D}^1$,

$$v = \sum_{k=1,2,..} a_k g_k \tag{39}$$

The dynamics of the coefficient a_k is given by taking the inner product of g_k with the left hand side of (36a):

$$\dot{a}_k + i\gamma a_k - \langle g_k, Lv \rangle = -\langle g_k, \dot{\tilde{u}} \rangle \tag{40}$$

$k=1,2,3,\ldots.$

By (36) and (37)

$$\langle g_k, Lv \rangle = \langle Lg_k, v \rangle = \varepsilon_k \langle g_k, v \rangle \tag{41}$$

so (40) becomes

$$\dot{a}_k + (i\gamma - \varepsilon_k)a_k = -\langle g_k, \dot{\tilde{u}} \rangle \tag{42a}$$

$k=1,2,3,\ldots$

The velocity profile w can now be computed as

$$u = \sum_{k=1,2,..} a_k g_k + \tilde{u} \tag{42b}$$

Observe that this system satisfies the boundary conditions *exactly* at each instant. Moreover, the approximation of (39) by a finite series can lead to inaccuracies only when $\jmath$ and τ_s vary in time. For steady $\jmath$ and τ_s, the solution is exact.

The problem with (42b) is that to compute $\tilde{u}$, $\jmath$ is needed. In view of intended applications of the model of vertical structure, forcing of the model by depth averaged velocity $\bar{u}$ would be preferable: in the context of current profile reconstruction from measurements, it is much easier to make a first guess of $\bar{u}$ than of $\jmath$, and in quasi 3D modeling, use of $\bar{u}$ is more accurate, since in this way, also depth averages of the nonlinear terms in the shallow water equation can be taken into account in the forcing.

Substitution of the solution (34) for $\tilde{u}$ in (42a) gives

$$\dot{a}_k + (i\gamma - \varepsilon_k)a_k = - < g_k, \, d/dt \, \beta_1 \jmath > - < g_k, \, d/dt \, \beta_2 \tau_s > \qquad (43)$$

$k=1,2,3,\ldots$

An expression for surface slope as a function of $\bar{u}$ and τ_s is obtained by substitution of (34) in (42b), and averaging over the water column:

$$\jmath = -\bar{\beta}_1^{-1}\Big[\sum_{k=1,2,..} a_k \bar{g}_k + \bar{\beta}_2 \tau_s - \bar{u} \Big] \qquad (44)$$

Insertion of (44) in (43) gives

$$\begin{aligned}
&\dot{a}_k + (i\gamma - \varepsilon_k)a_k = \\
&- < g_k, \, \dot{\beta}_2 > \tau_s - < g_k, \, \beta_2 > \dot{\tau}_s \\
&+ < g_k, \, d/dt(\bar{\beta}_1^{-1}\beta_1) > \Big[\sum_{j=1,2,..} a_j \bar{g}_j + \bar{\beta}_2 \tau_s - \bar{u} \Big] \\
&+ < g_k, \, \bar{\beta}_1^{-1}\beta_1 > \Big[\sum_{j=1,2,..} \dot{a}_j \bar{g}_j + \dot{\bar{\beta}}_2 \tau_s + \bar{\beta}_2 \dot{\tau}_s - \dot{\bar{u}} \Big] \qquad (45)
\end{aligned}$$

After rearranging terms, the following system of equations is obtained:

$$[I - \mathbf{c}\mathbf{d}^T]\dot{\mathbf{a}} = [\Lambda + \dot{\mathbf{c}}\mathbf{d}^T]\mathbf{a} + B\dot{\mathbf{b}} + \dot{B}\mathbf{b} \qquad (46a)$$

with $\mathbf{a} \triangleq (a_1, a_2, \ldots)^T$ and $\mathbf{c}$ and $\mathbf{d}$ vectors with components

$$c_k \triangleq < g_k, \, \bar{\beta}_1^{-1}\beta_1 > \quad \text{and} \quad d_k \triangleq \bar{g}_j \qquad (46b)$$

Λ diagonal, with $\lambda_{kk} = \varepsilon_k - i\gamma$ (46c)

$\mathbf{b} \triangleq (\tau_s \quad \bar{u})^T$ (46d)

$B_{k,i}$ (row k and column i of the matrix B) is given by

$$B_{k,1} = < g_k, \beta_1 > \bar{\beta}_1^{-1} \bar{\beta}_2 - < g_k, \beta_2 > \quad (46e)$$

$$B_{k,2} = - < g_k, \beta_1 > \bar{\beta}_1^{-1} \quad (46f)$$

Probably the best method for solving (46a) is to solve the equivalent discrete system, obtained by assuming that all model parameters and inputs are linear functions of time between the instants at which they are given, and then writing down the analytical solution of the linear system for **a**. The solution involves matrix exponents. Numerical exponentiation of matrices can be avoided, due to the simple structure of the matrices involved (rank-2 modifications of diagonal matrices). Nevertheless, the numerical solution still requires a considerable number of (scalar) exponents, which are expensive.

An alternative approach is to use simple finite differencing both for inputs and parameters, and for the evolution of the state **a** itself. This may require smaller time steps, but the amount of computation per time step is smaller. Moreover, the method is more general, in the sense that if the system of equations is modified to a truly nonlinear implicit system of equations, the integration method can still be applied.
(46) can be initialized by setting **a** equal to zero. Inserting (34) in (42b) and using (44), we obtain for u:

$$u = \sum_{k=1,2,..} [g_k - \bar{g}_k \bar{\beta}_1^{-1} \beta_1] a_k + [\beta_2 - \bar{\beta}_2 \bar{\beta}_1^{-1} \beta_1] \tau_s + [\bar{\beta}_1^{-1} \beta_1] \bar{u} \quad (46g)$$

As in appendix a1, this can be worked out analytically for the case of a uniform eddy viscosity. Numerical approximation of the basis $\{g_k, k=1,2,..\}$ is possible in principle for other kind of eddy viscosity profile shapes, by solving the corresponding eigenvalue problem.

DELFT HYDRAULICS

CURRENT VELOCITY
manning 0.027

H 972 | 14-11-90

FIG. 1a | VERSIE 1.1

88-11-17

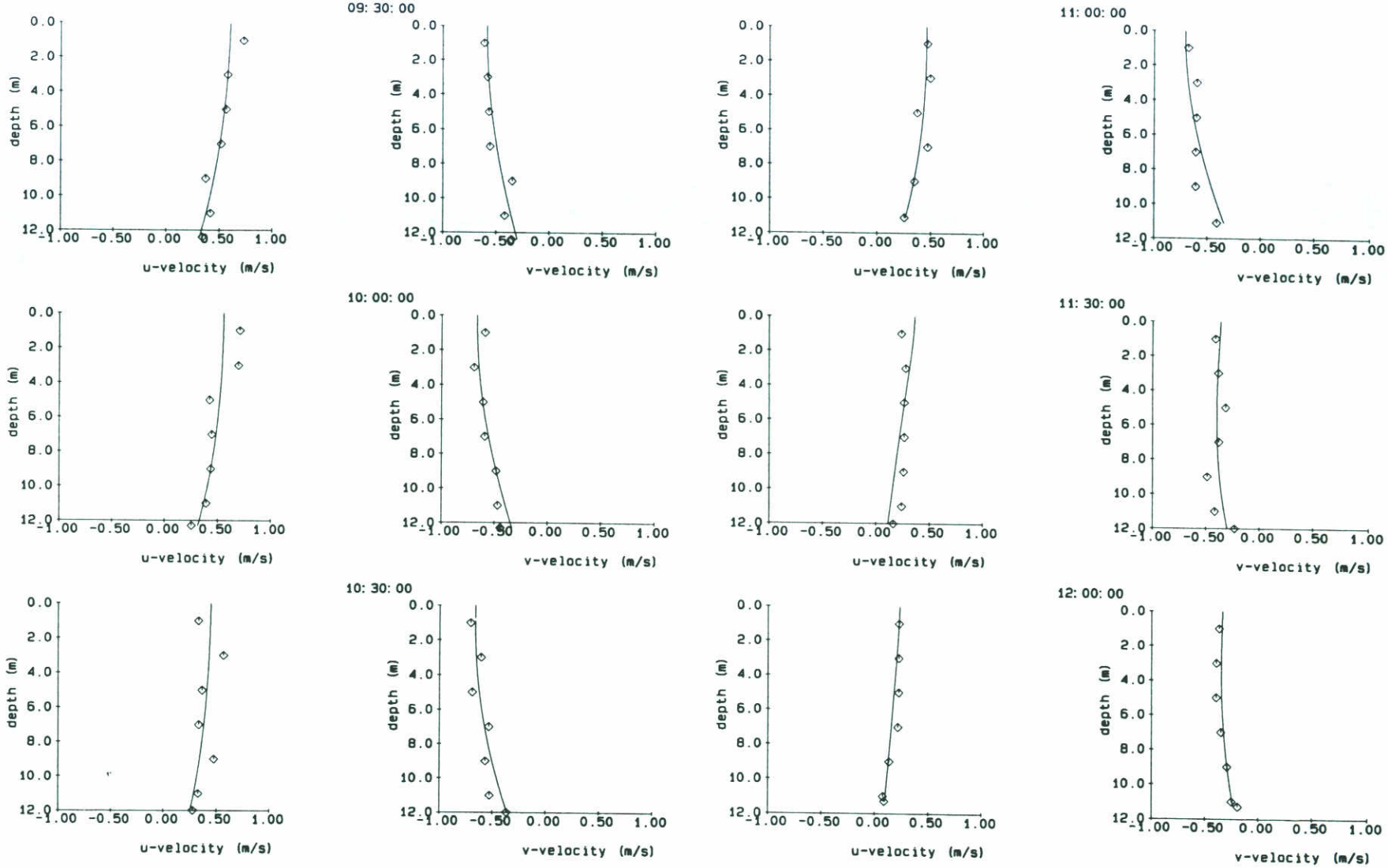

DELFT HYDRAULICS

CURRENT VELOCITY
manning 0.027

H 972

VERSIE 1.1

14-11-90

FIG. 1b

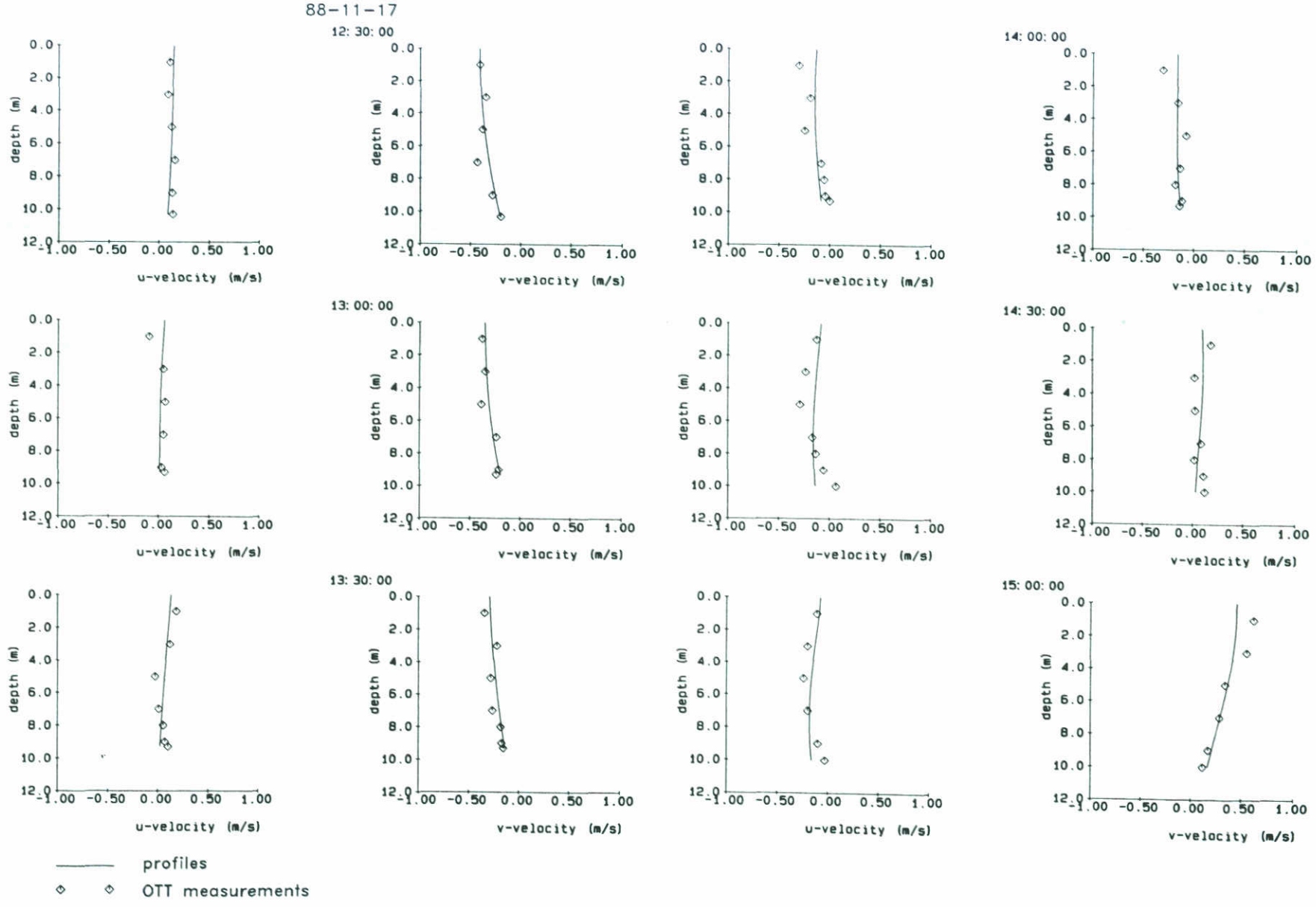

DELFT HYDRAULICS

CURRENT VELOCITY

manning 0.027

88-11-17

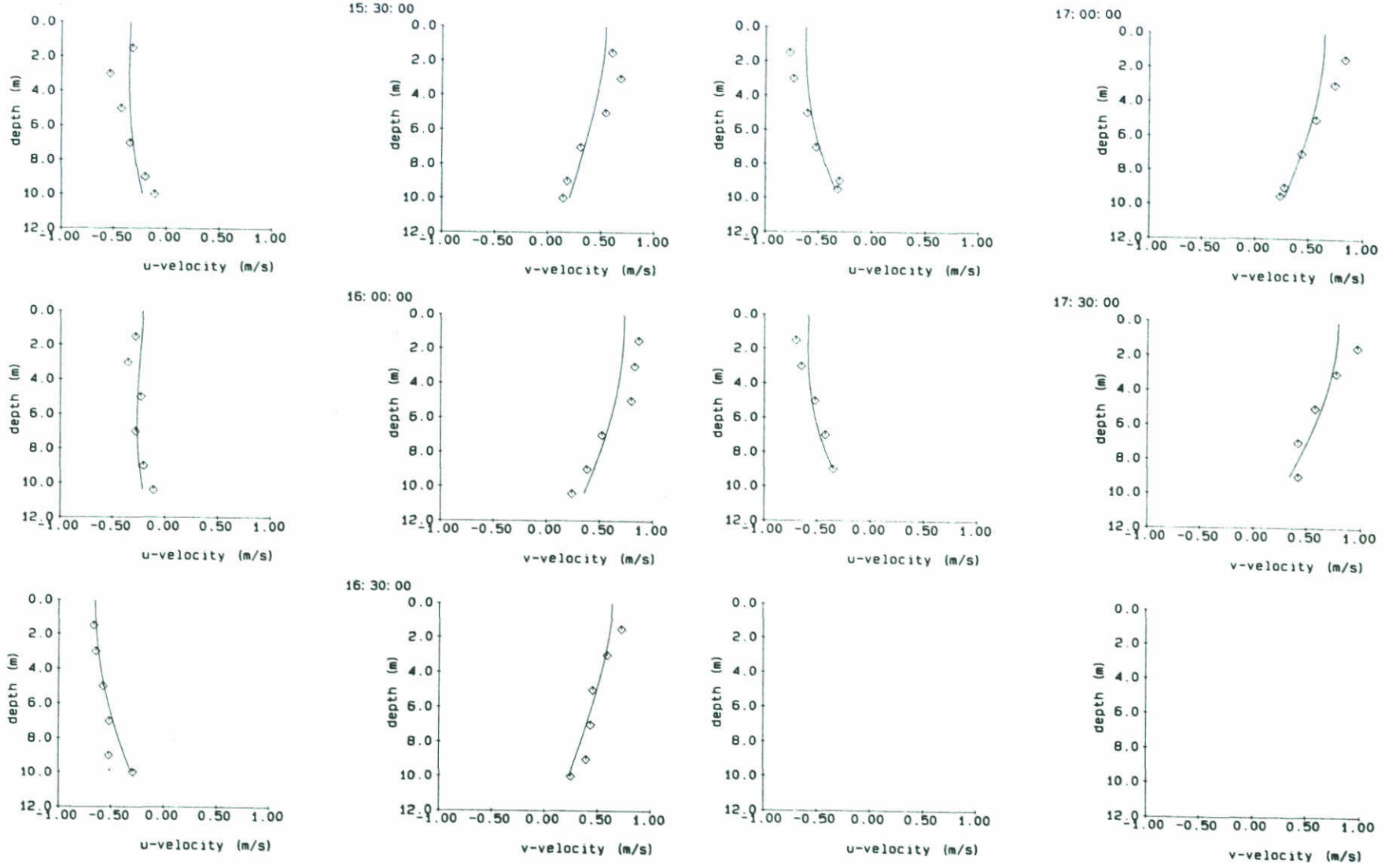

H 972	VERSIE 1.1	14-11-90
FIG. 1c		

DELFT HYDRAULICS

CURRENT VELOCITY
TT8

H 972

VERSIE 1.1

14-11-90

FIG. 2a

88-11-17

09: 30: 00

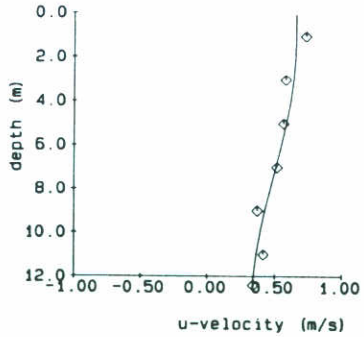

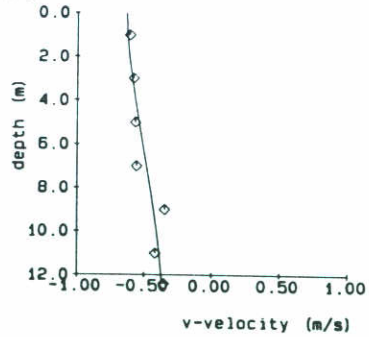

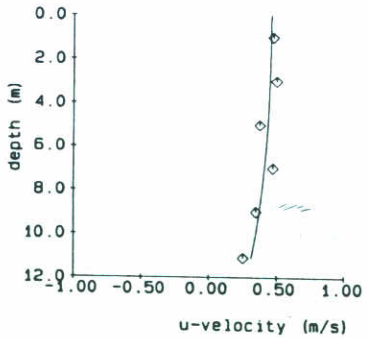

11: 00: 00

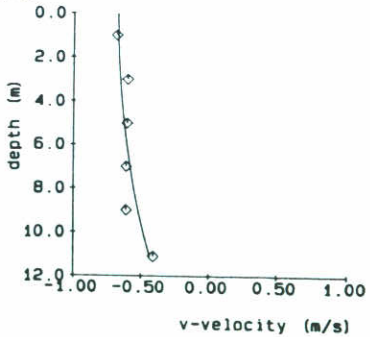

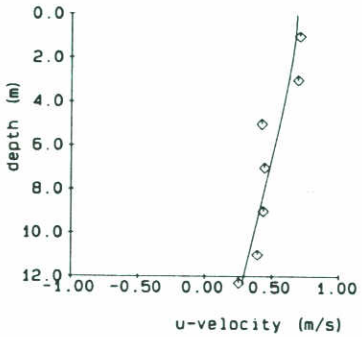

10: 00: 00

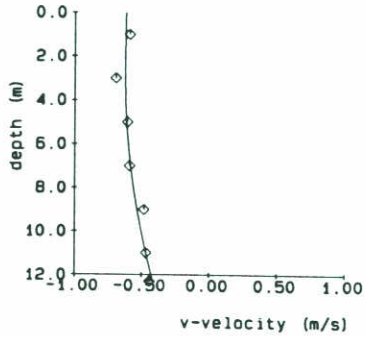

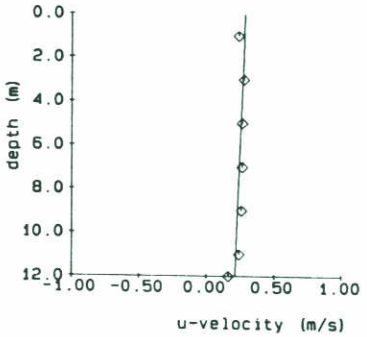

11: 30: 00

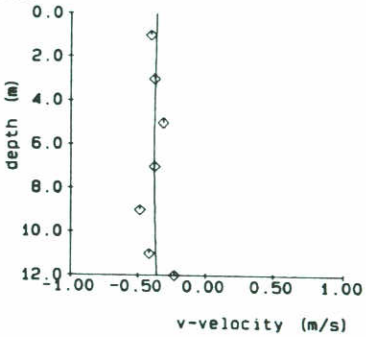

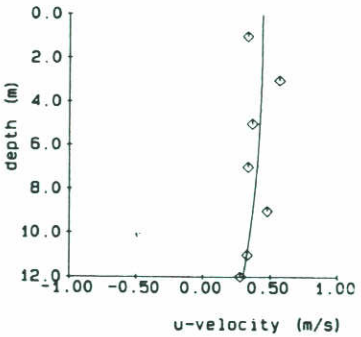

10: 30: 00

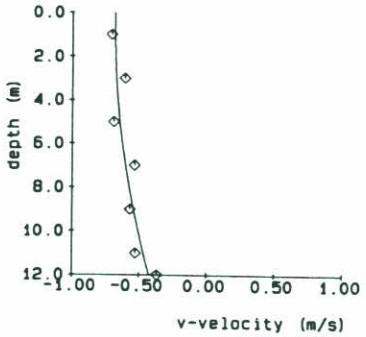

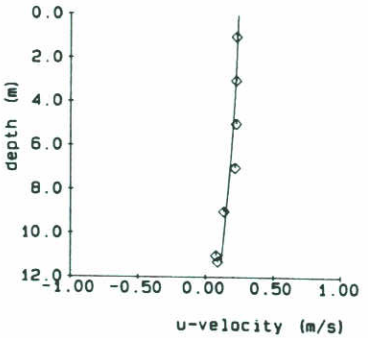

12: 00: 00

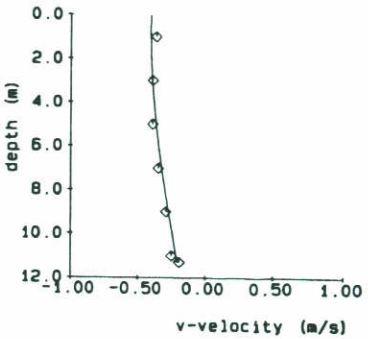

profiles

OTT measurements

88-11-17

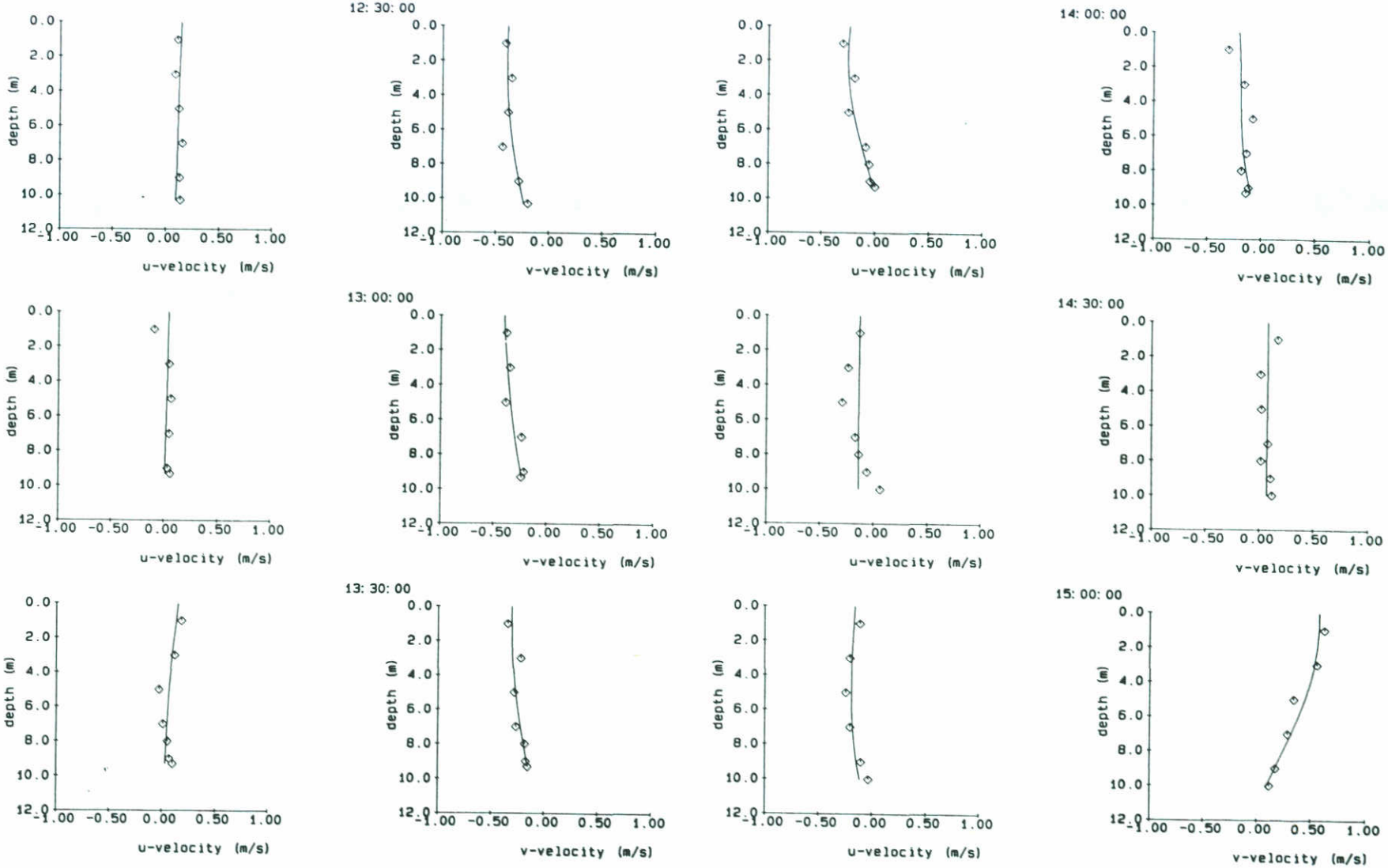

CURRENT VELOCITY
TT8

DELFT HYDRAULICS

14-11-90

VERSIE 1.1

H 972

FIG. 2b

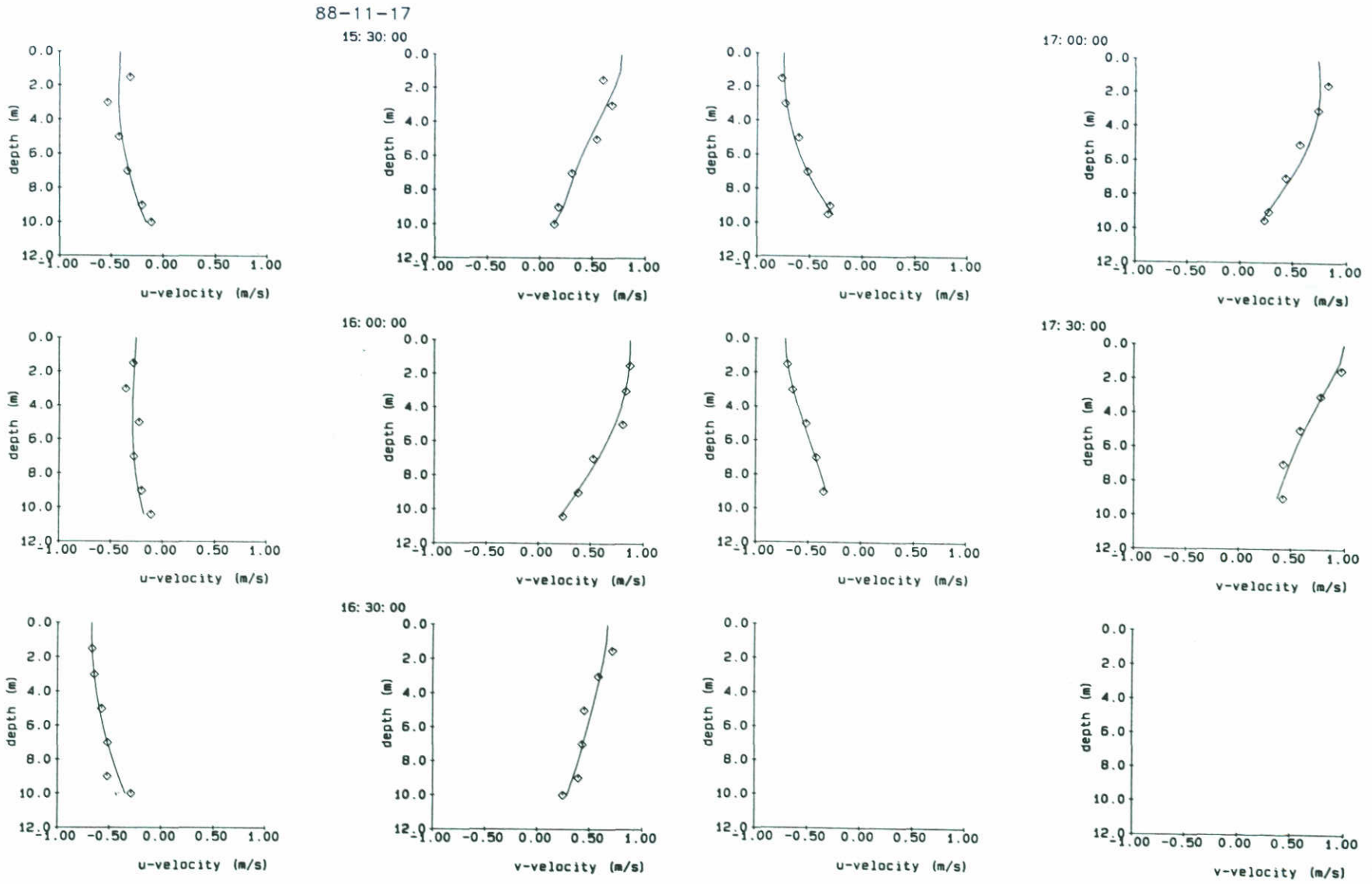

DELFT HYDRAULICS

CURRENT VELOCITY
TT8

H 972

VERSIE 1.1

14-11-90

FIG. 2c

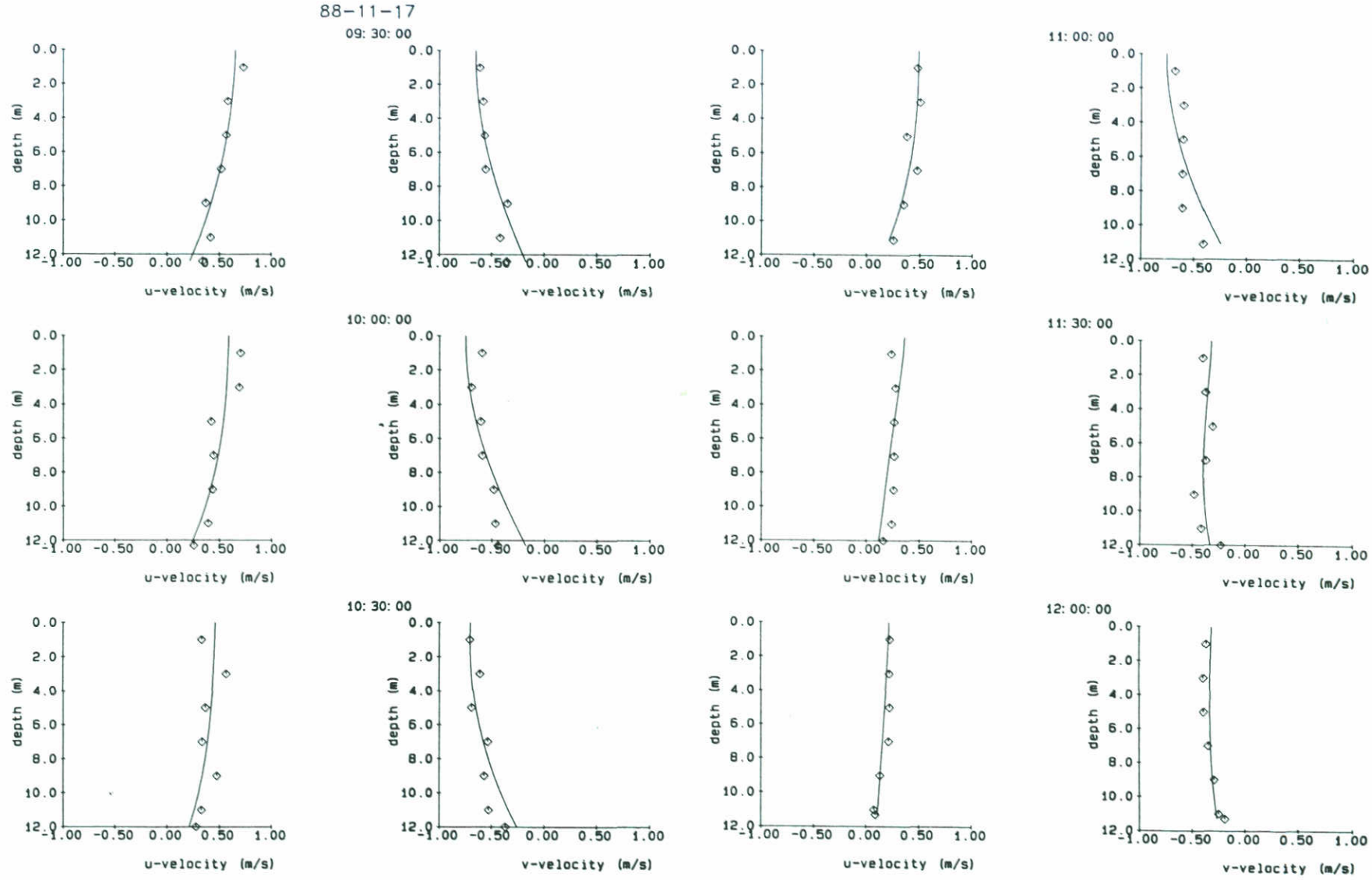

DELFT HYDRAULICS

CURRENT VELOCITY
TT4

14-11-90

VERSIE 1.1

H 972

FIG. 3a

DELFT HYDRAULICS

CURRENT VELOCITY
TT4

H 972

VERSIE 1.1

14-11-90

FIG. 3b

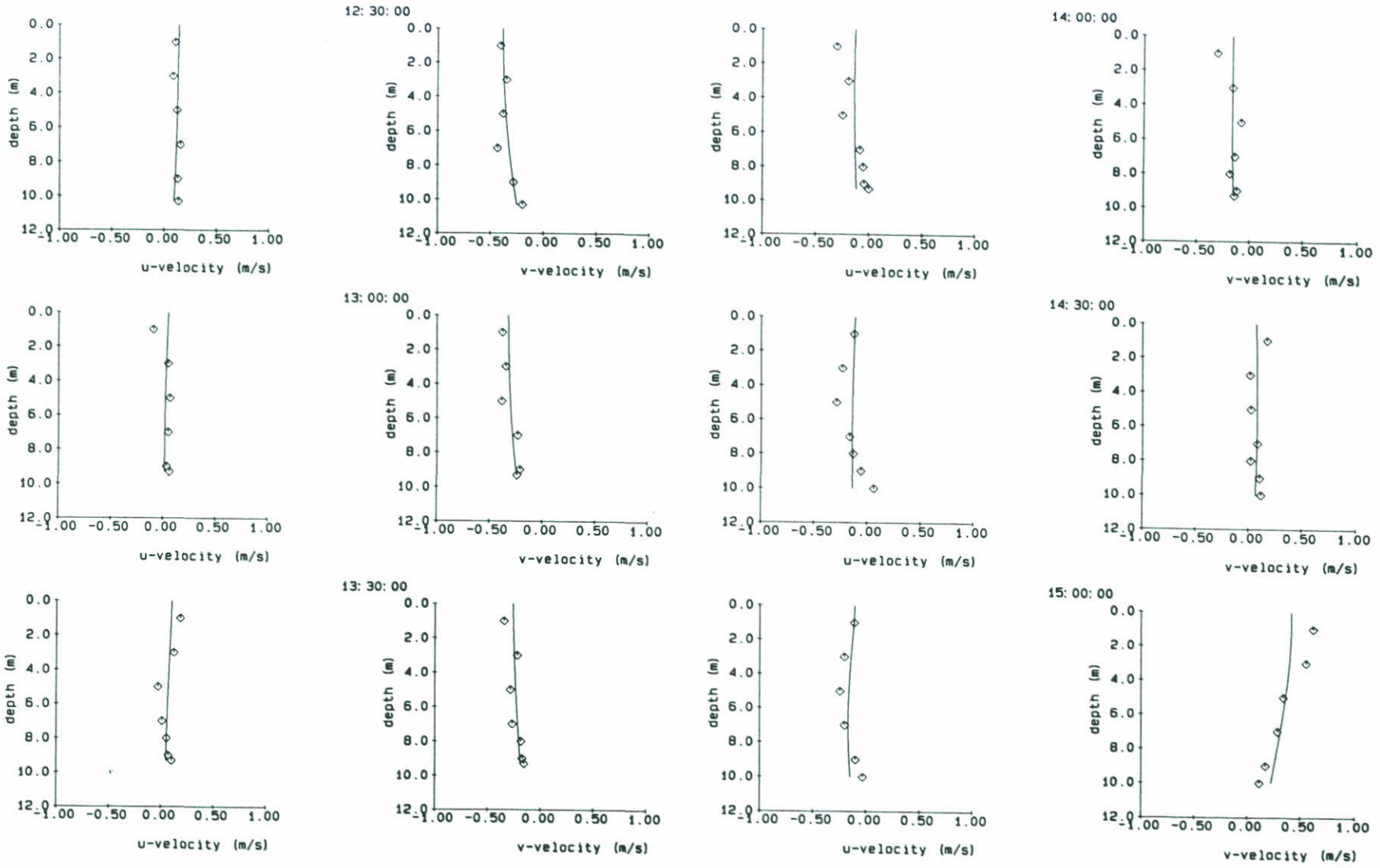

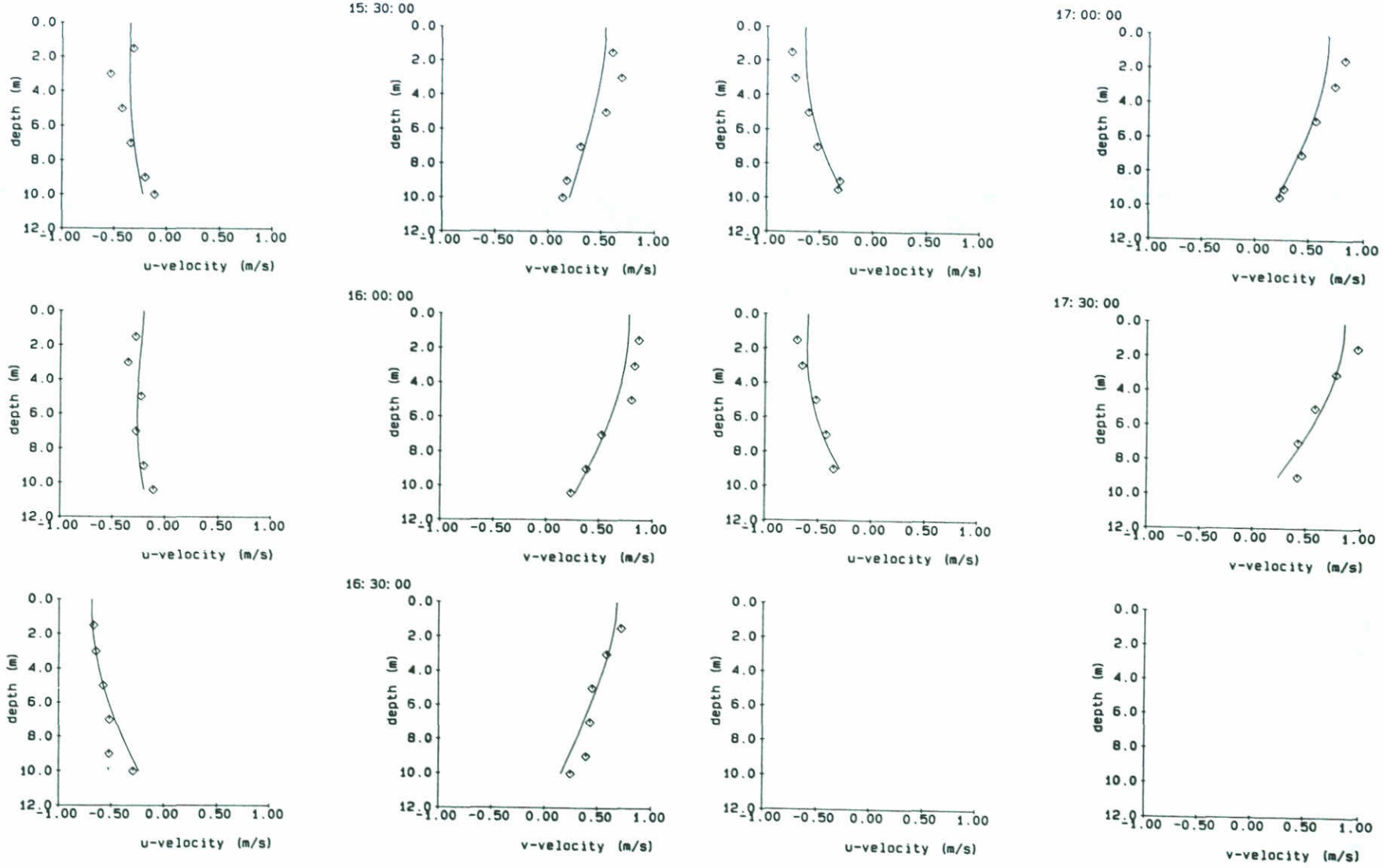

CURRENT VELOCITY
TT4

DELFT HYDRAULICS

14-11-90

VERSIE 1.1

H 972

FIG. 3c

DELFT HYDRAULICS

CURRENT VELOCITY
TT5

H 972

VERSIE 1.1

14-11-90

FIG. 4a

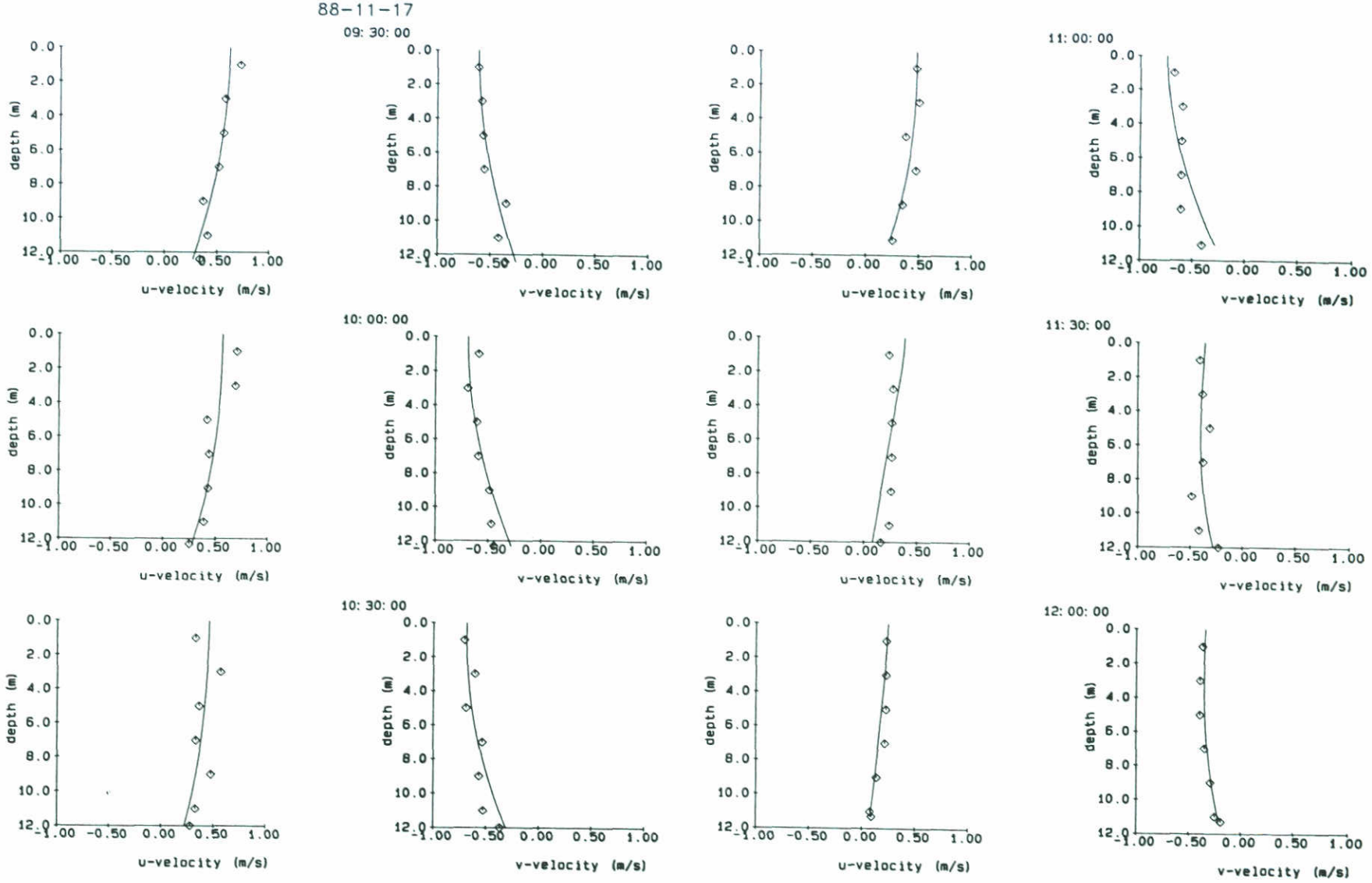

DELFT HYDRAULICS

CURRENT VELOCITY
TT5

VERSIE 1.1

14-11-90

H 972

FIG. 4b

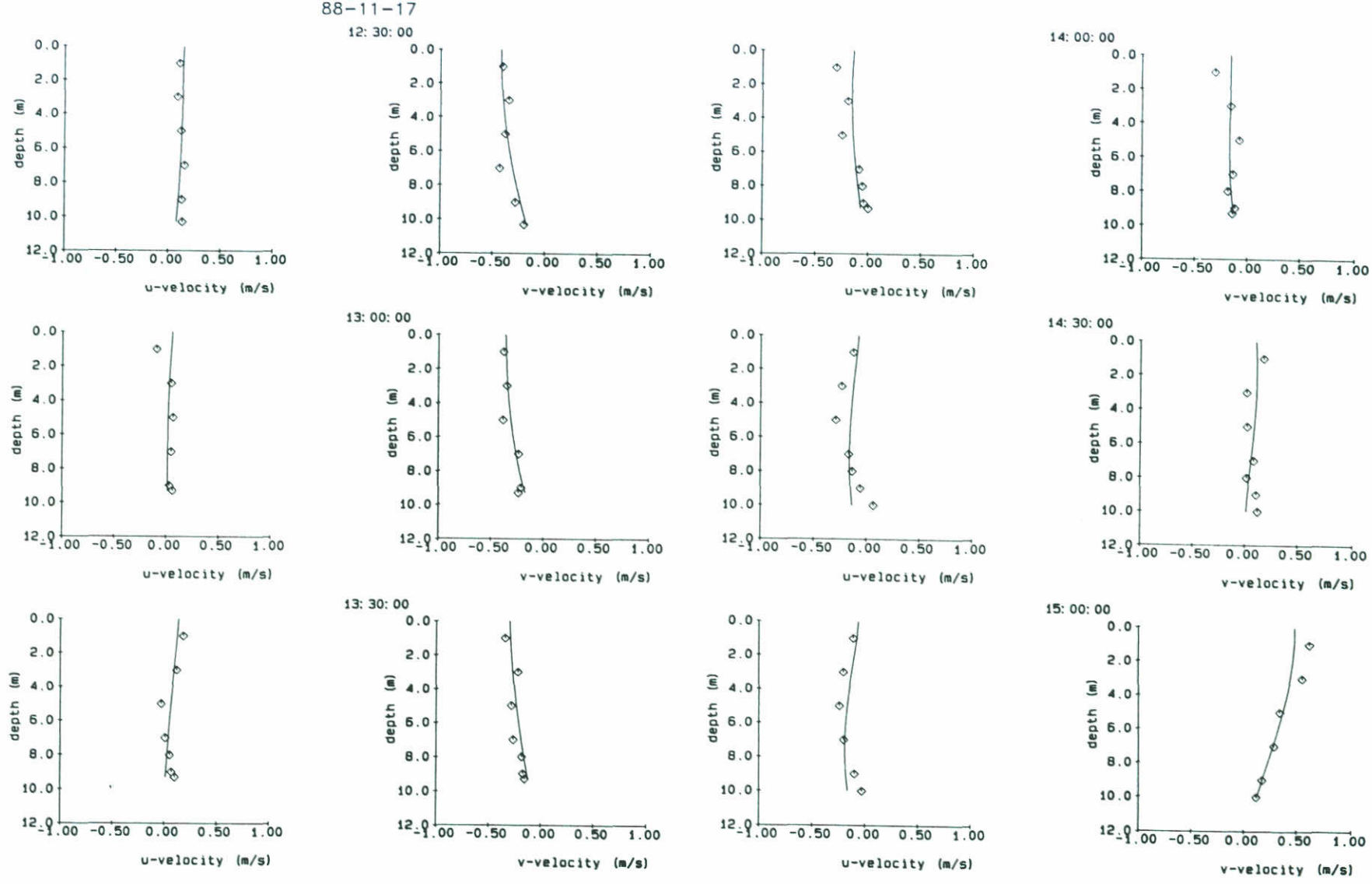

DELFT HYDRAULICS

CURRENT VELOCITY

TT5

H 972

VERSIE 1.1

14-11-90

FIG. 4c

88-11-17

15: 30: 00

16: 00: 00

16: 30: 00

17: 00: 00

17: 30: 00

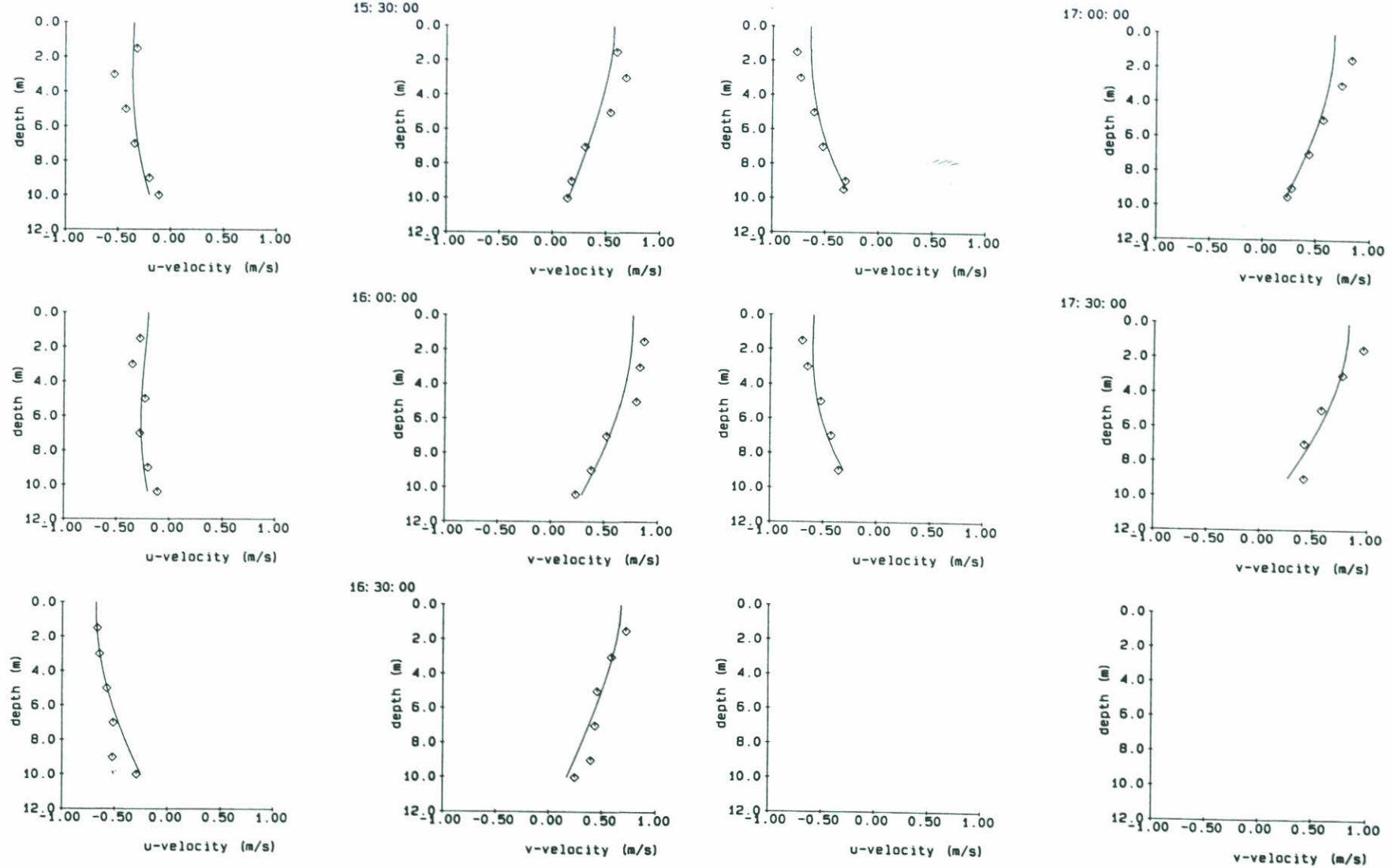

DELFT HYDRAULICS

CURRENT VELOCITY
TT6

14-11-90

VERSIE 1.1

H 972

FIG. 5a

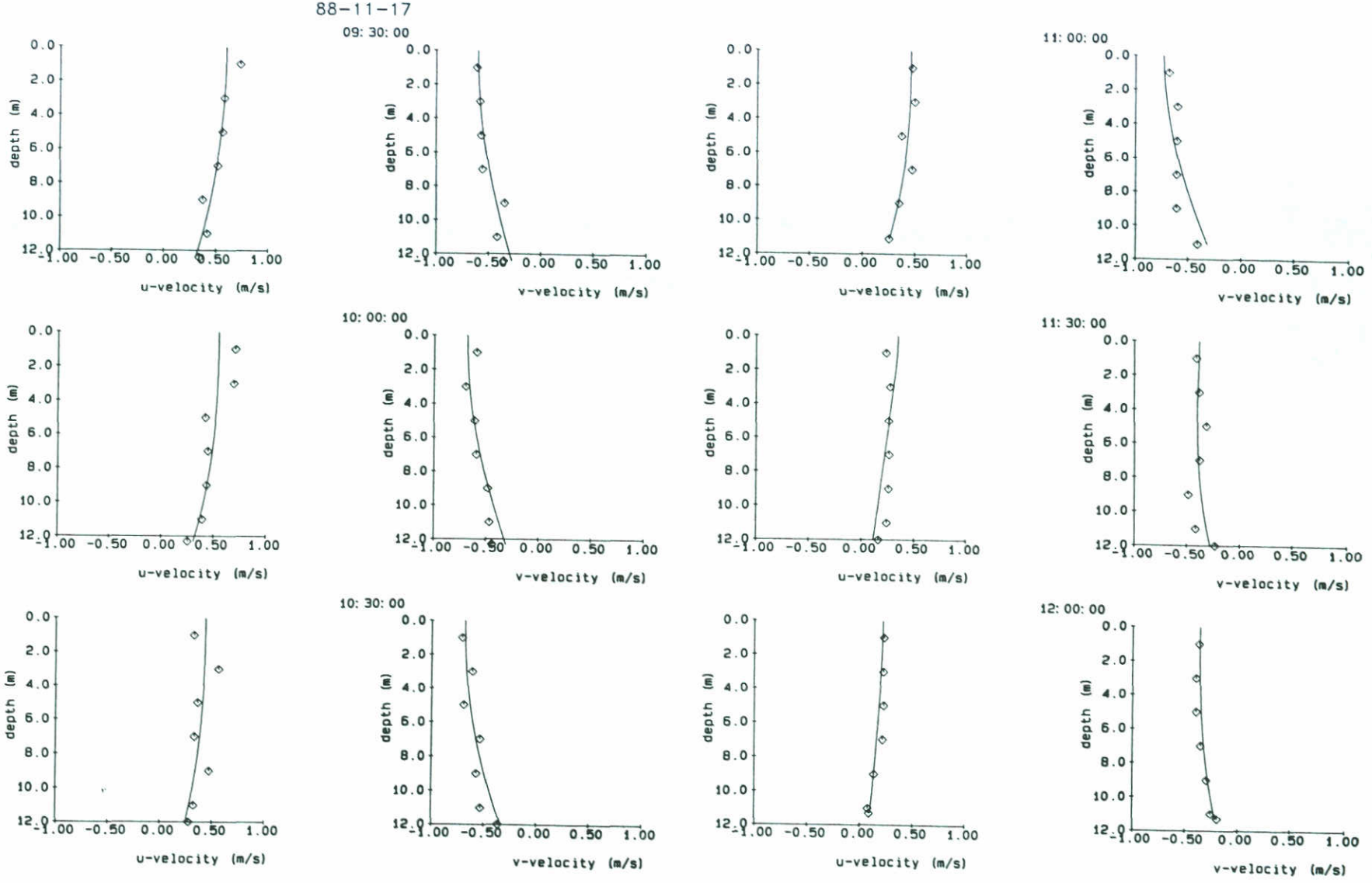

DELFT HYDRAULICS

CURRENT VELOCITY
TT6

H 972

VERSIE 1.1

14-11-90

FIG. 5b

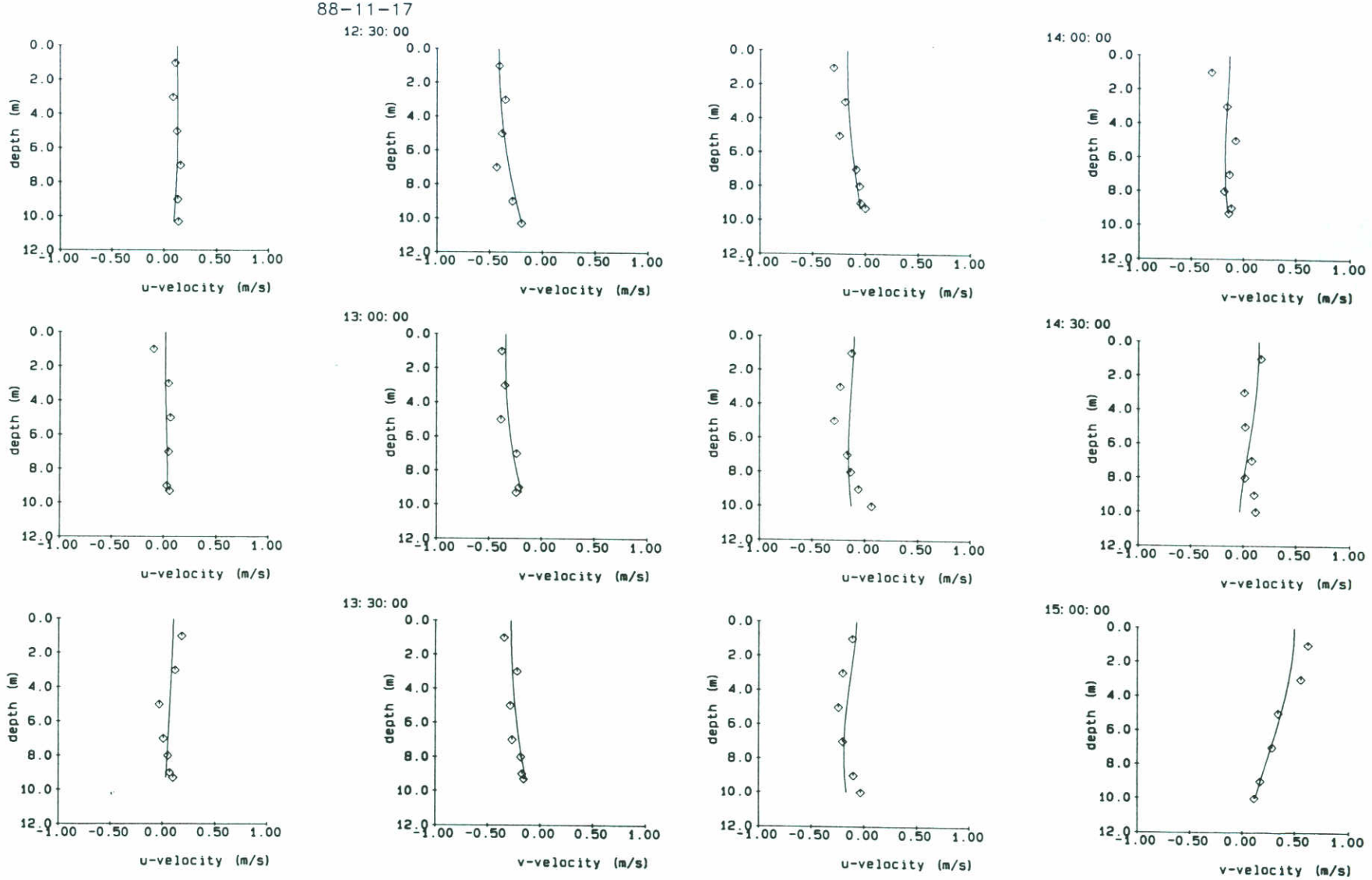

DELFT HYDRAULICS

CURRENT VELOCITY
TT6

H 972 | VERSIE 1.1 | 14-11-90

FIG. 5c

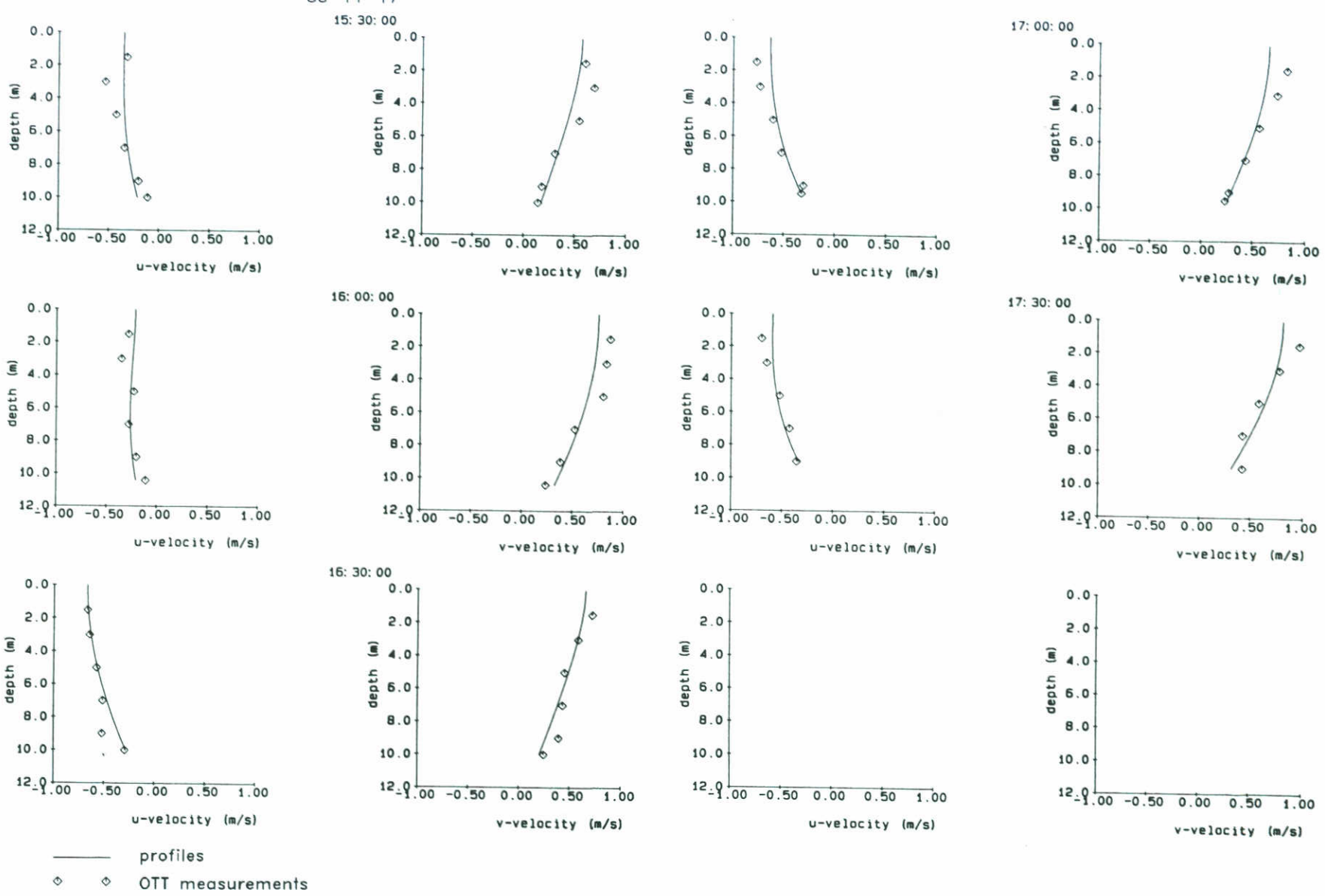

DELFT HYDRAULICS

CURRENT VELOCITY
TT7

H 972

VERSIE 1.1

14-11-90

FIG. 6a

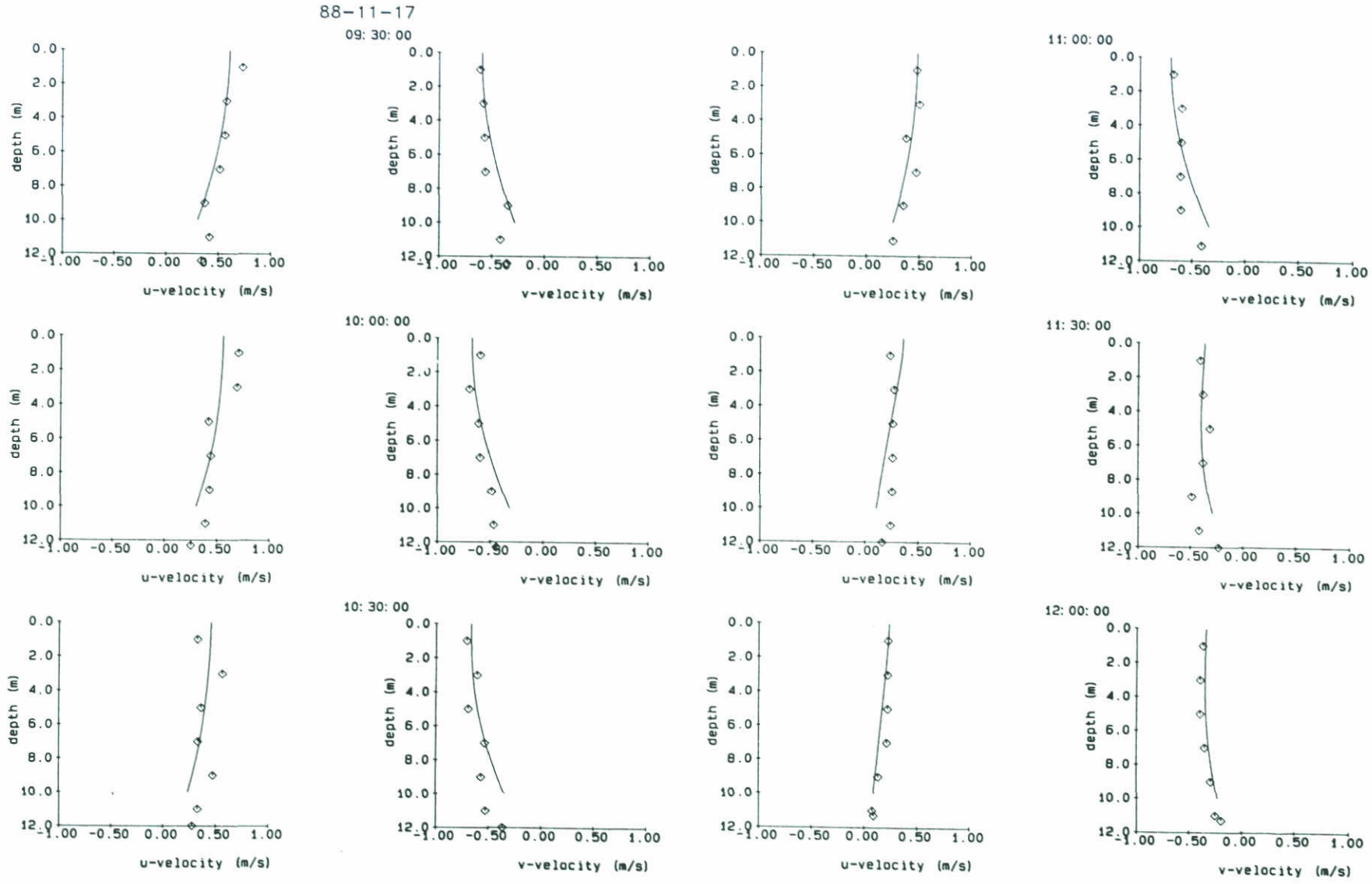

DELFT HYDRAULICS

CURRENT VELOCITY
TT7

H 972

VERSIE 1.1

14-11-90

FIG. 6b

88-11-17

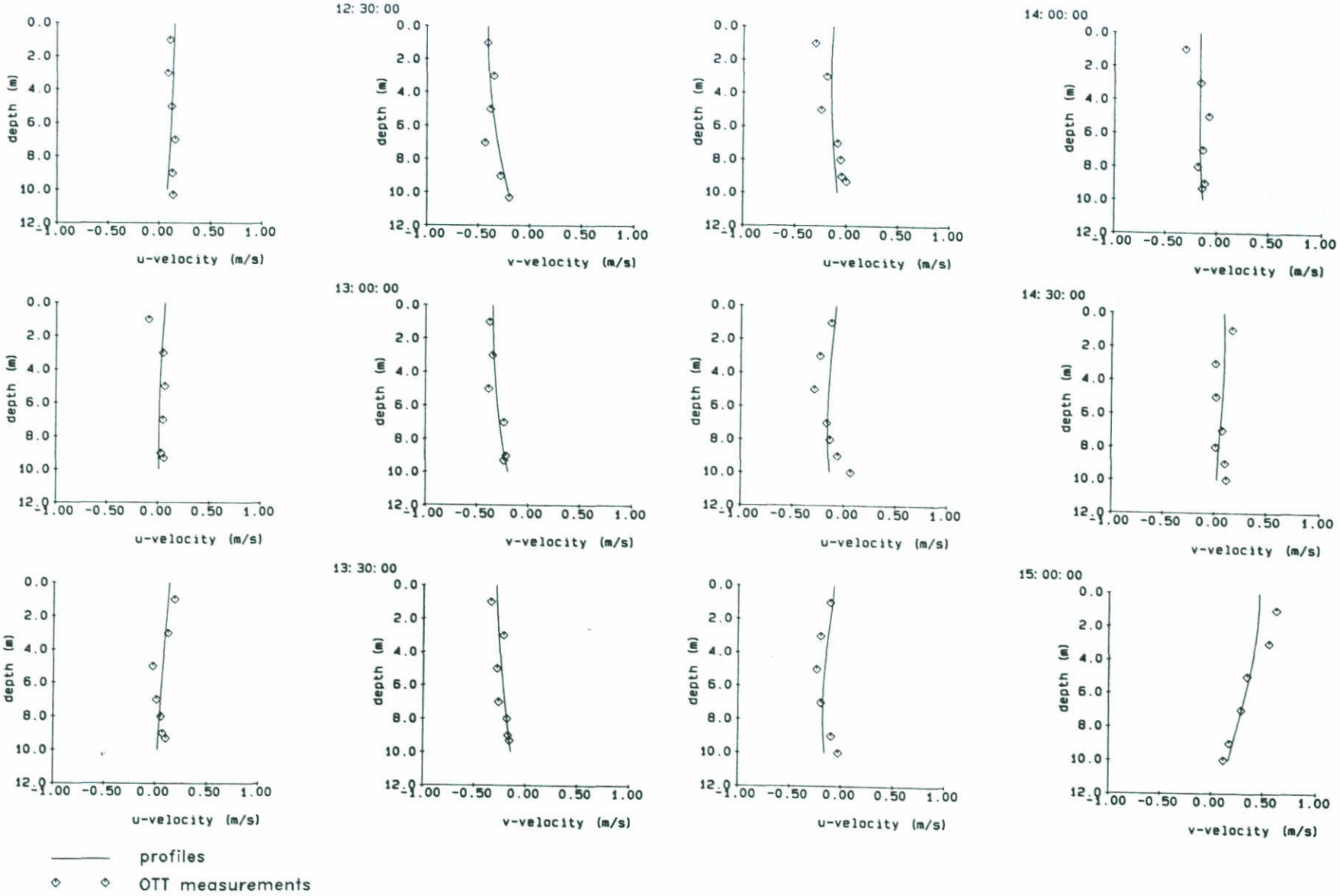

DELFT HYDRAULICS

CURRENT VELOCITY
TT7

14-11-90

VERSIE 1.1

H 972

FIG. 6c

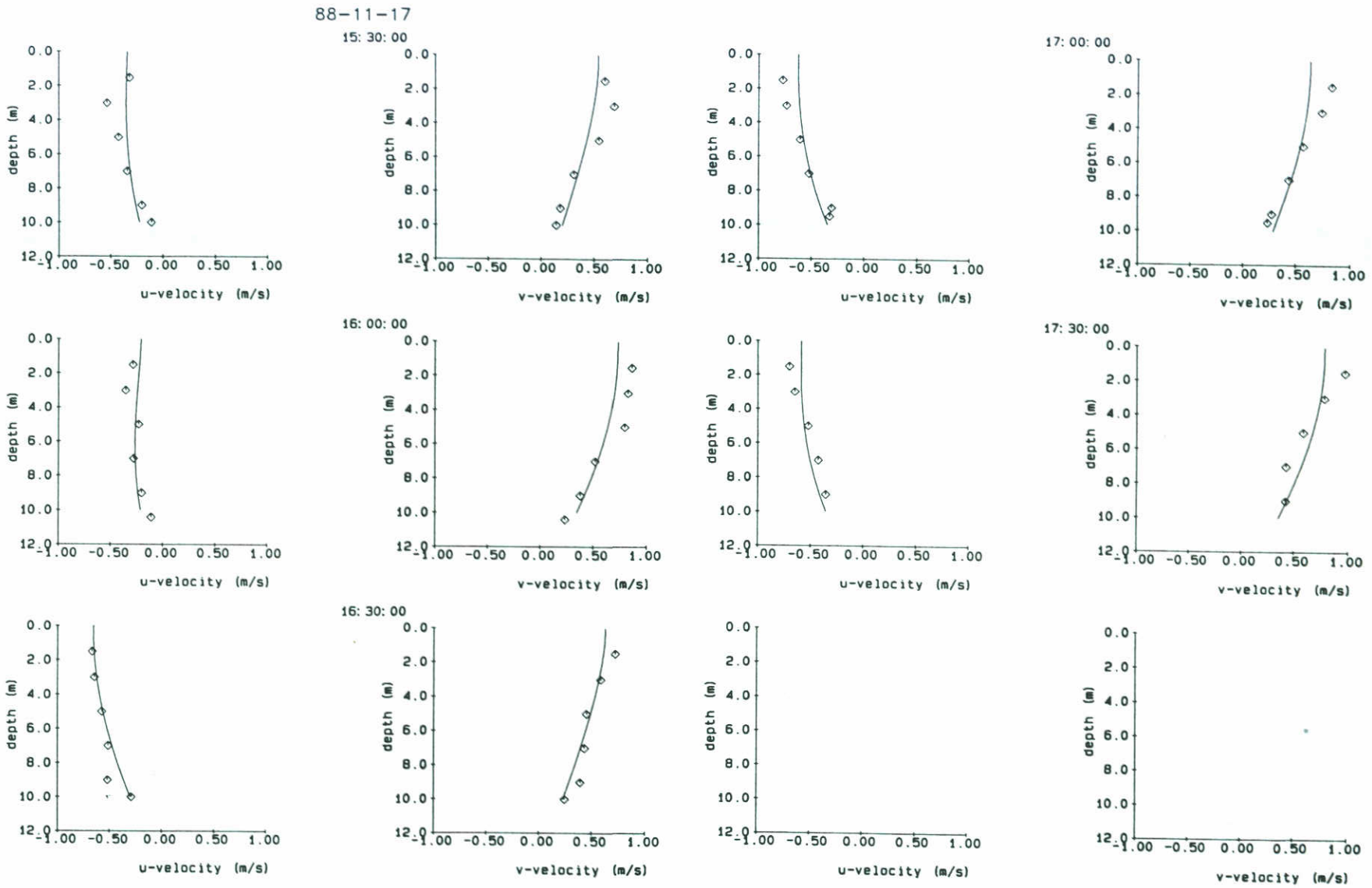

DELFT HYDRAULICS

CURRENT VELOCITY
TT3

VERSIE 1.1

14-11-90

H 972

FIG. 7a

88-11-17

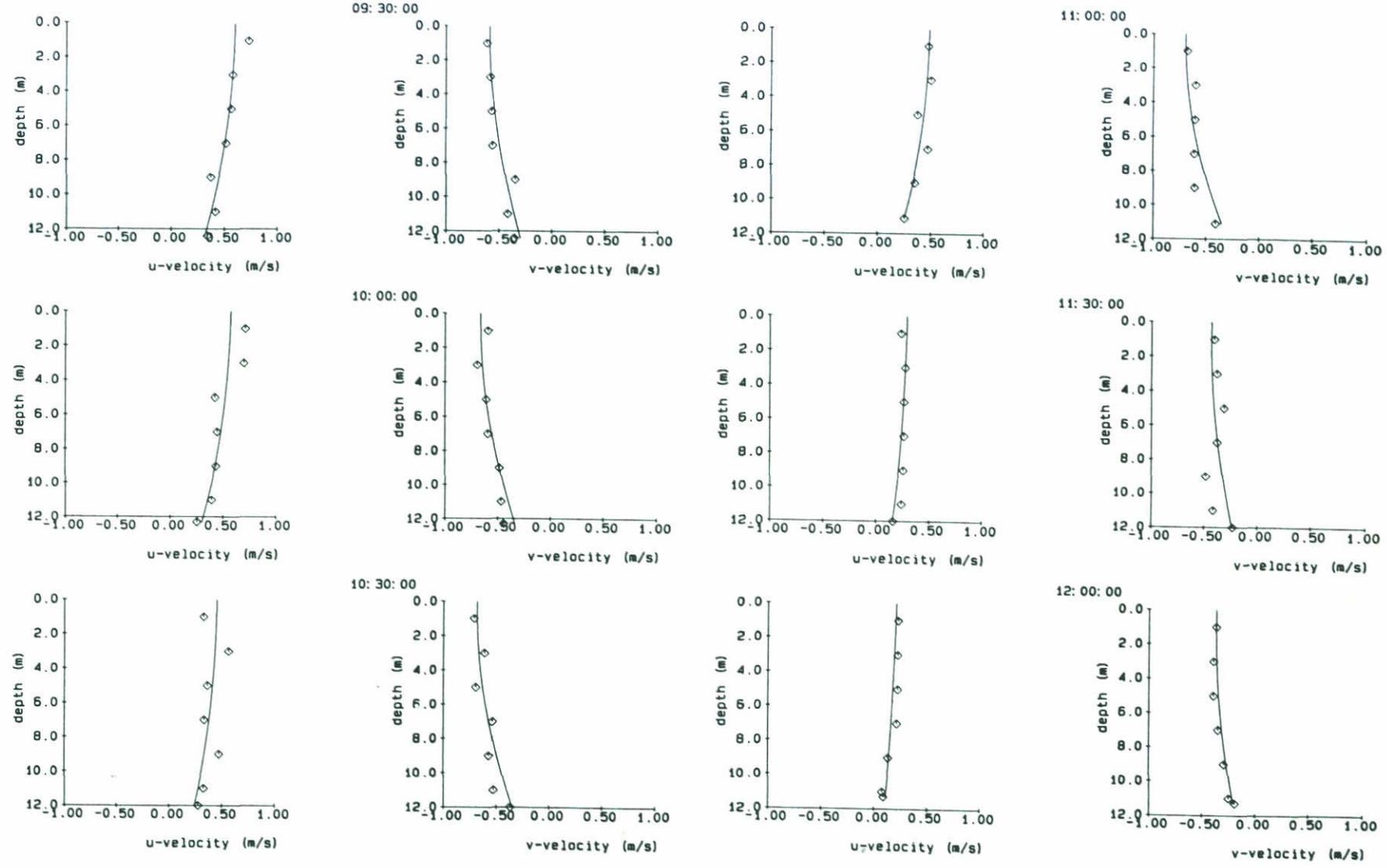

88-11-17

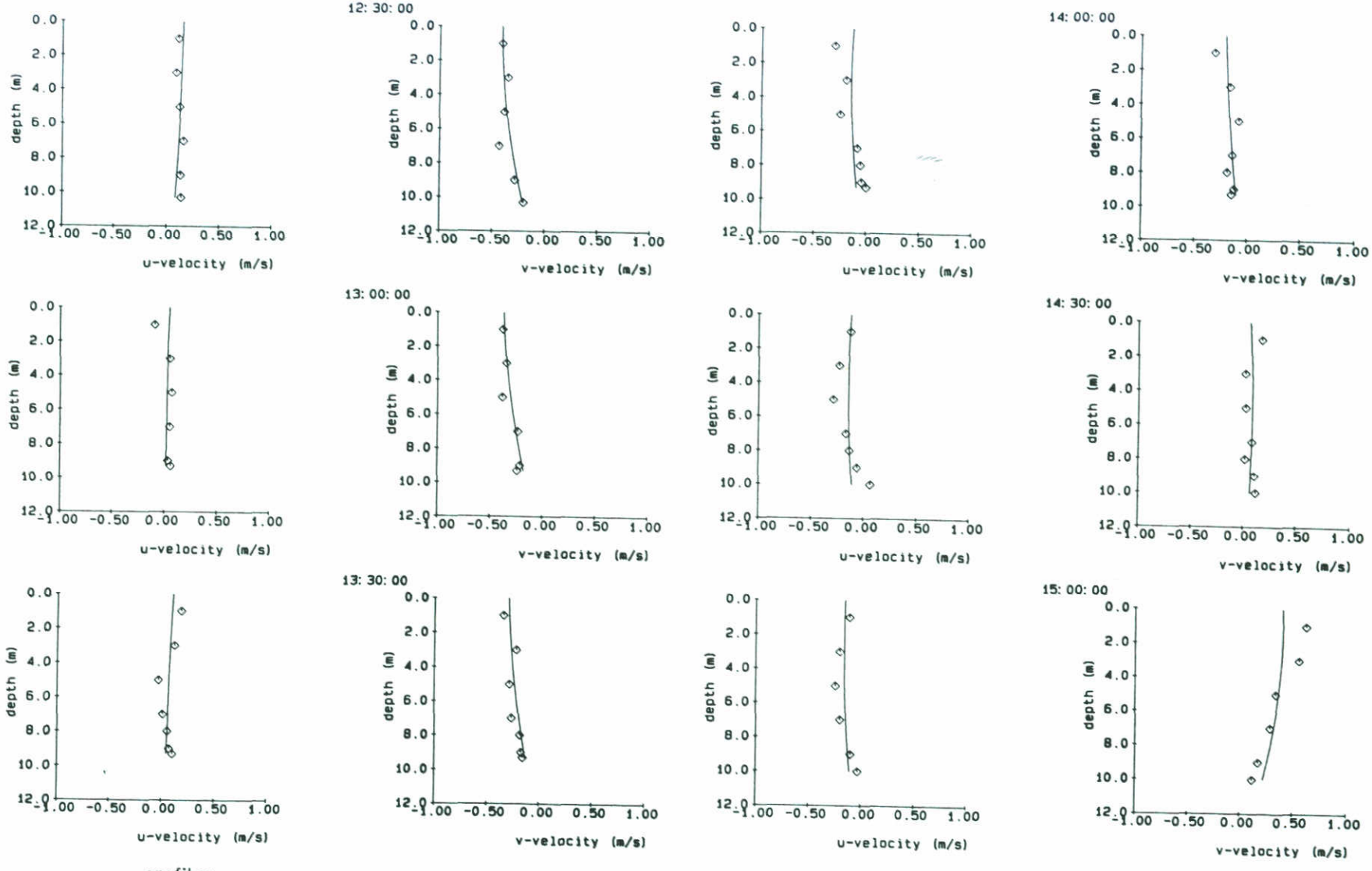

CURRENT VELOCITY
TT3

DELFT HYDRAULICS

14-11-90

VERSIE 1.1

H 972

FIG. 7b

DELFT HYDRAULICS

CURRENT VELOCITY
TT3

H 972 | VERSIE 1.1 | 14-11-90

FIG. 7c

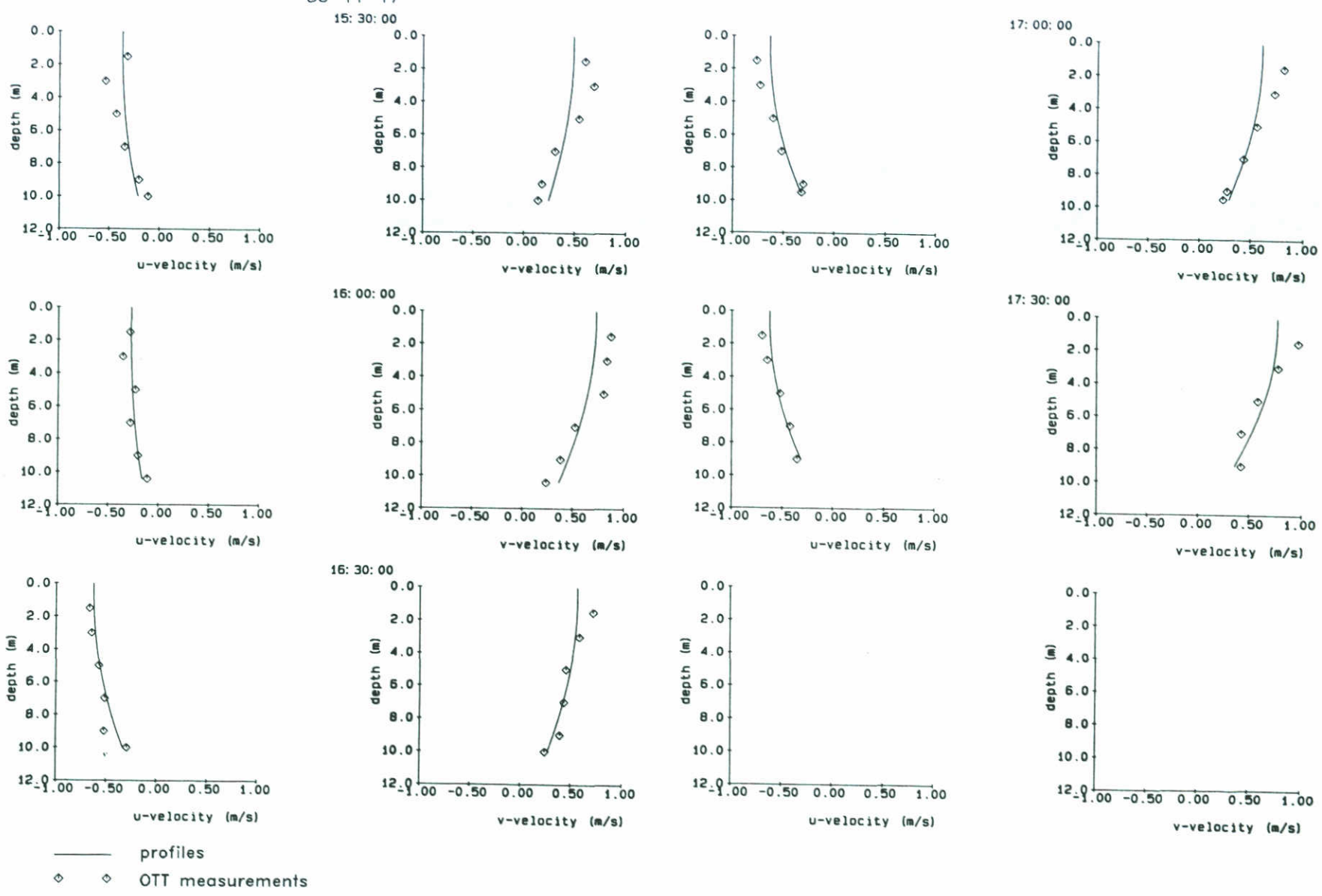

DELFT HYDRAULICS

CURRENT VELOCITY
HF6

H 972

VERSIE 1.1

14-11-90

FIG. 8a

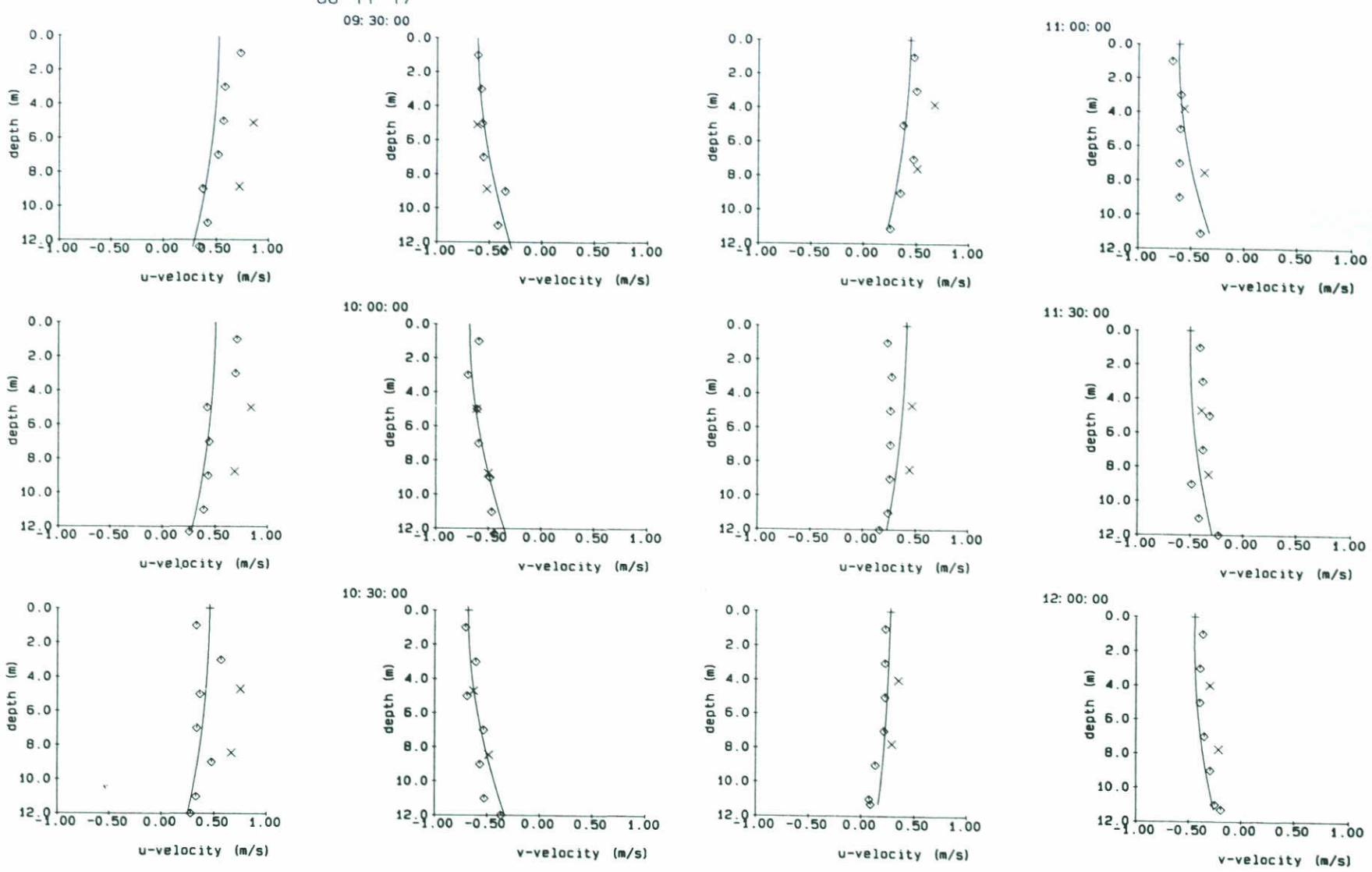

DELFT HYDRAULICS

CURRENT VELOCITY
HF6

H 972

VERSIE 1.1

14-11-90

FIG. 8b

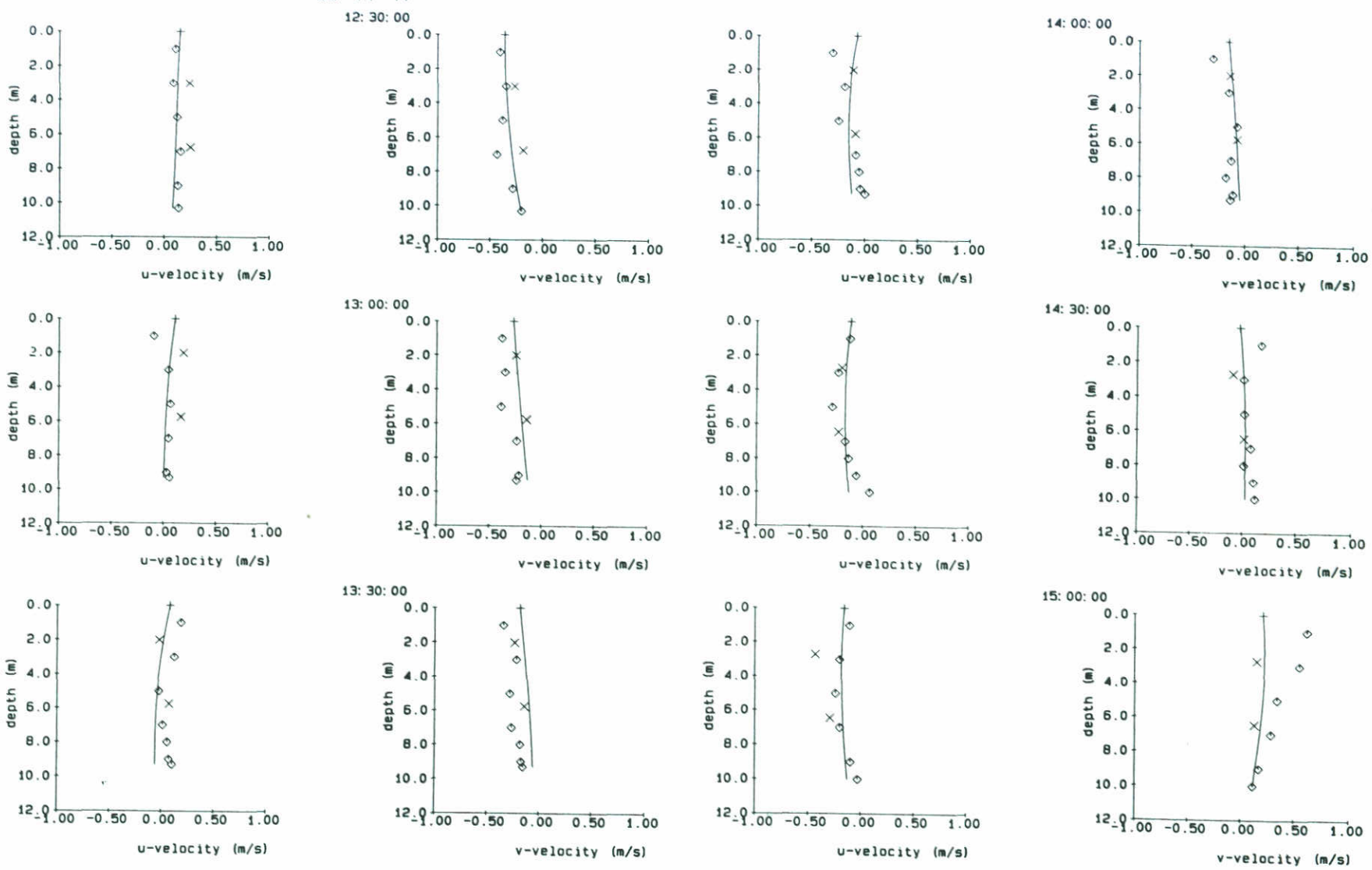

DELFT HYDRAULICS

CURRENT VELOCITY
HF6

H 972 | VERSIE 1.1 | 14-11-90

FIG. 8c

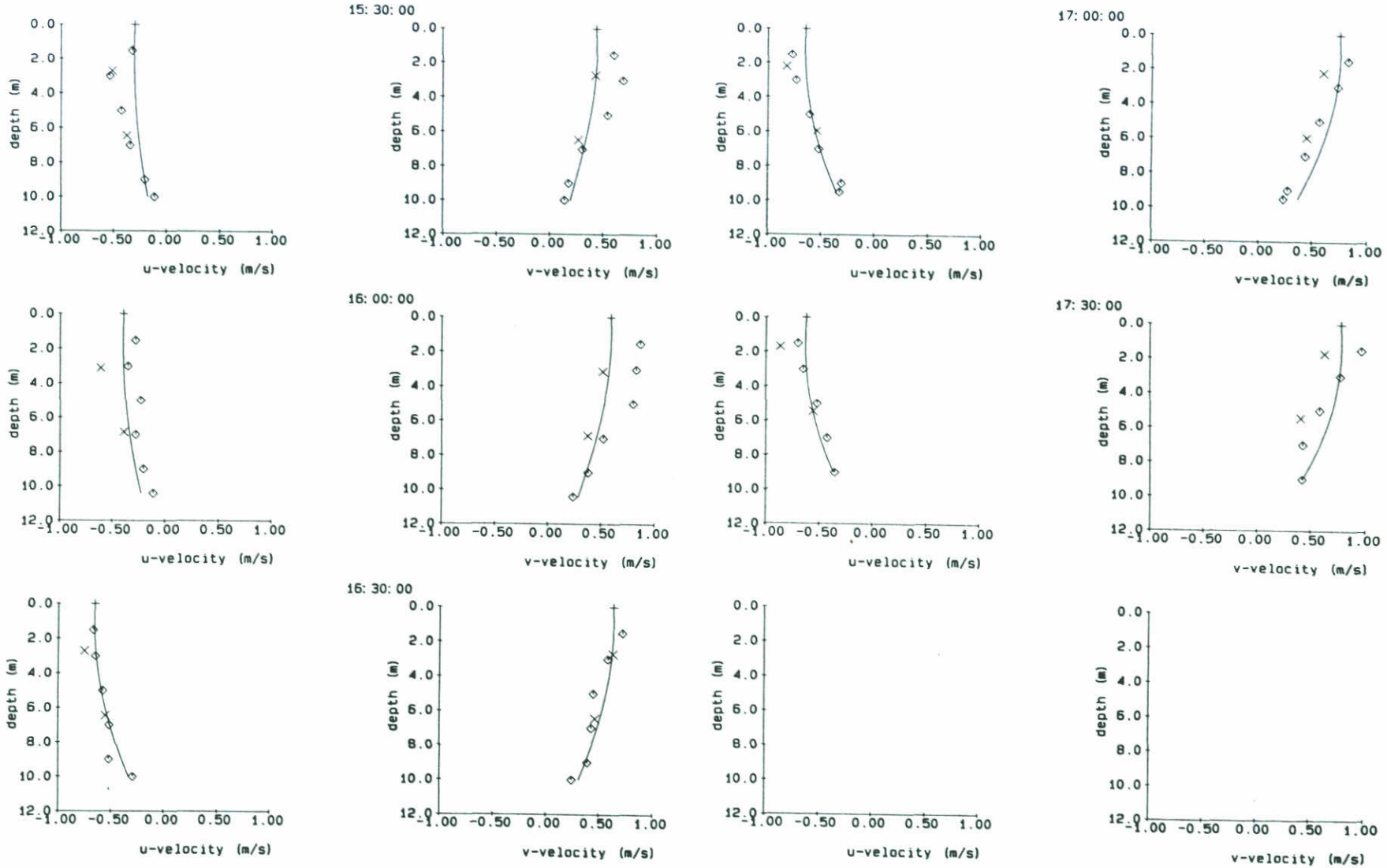

DELFT HYDRAULICS

CURRENT VELOCITY
HF6

H 972

VERSIE 1.1

14-11-90

FIG. 9a

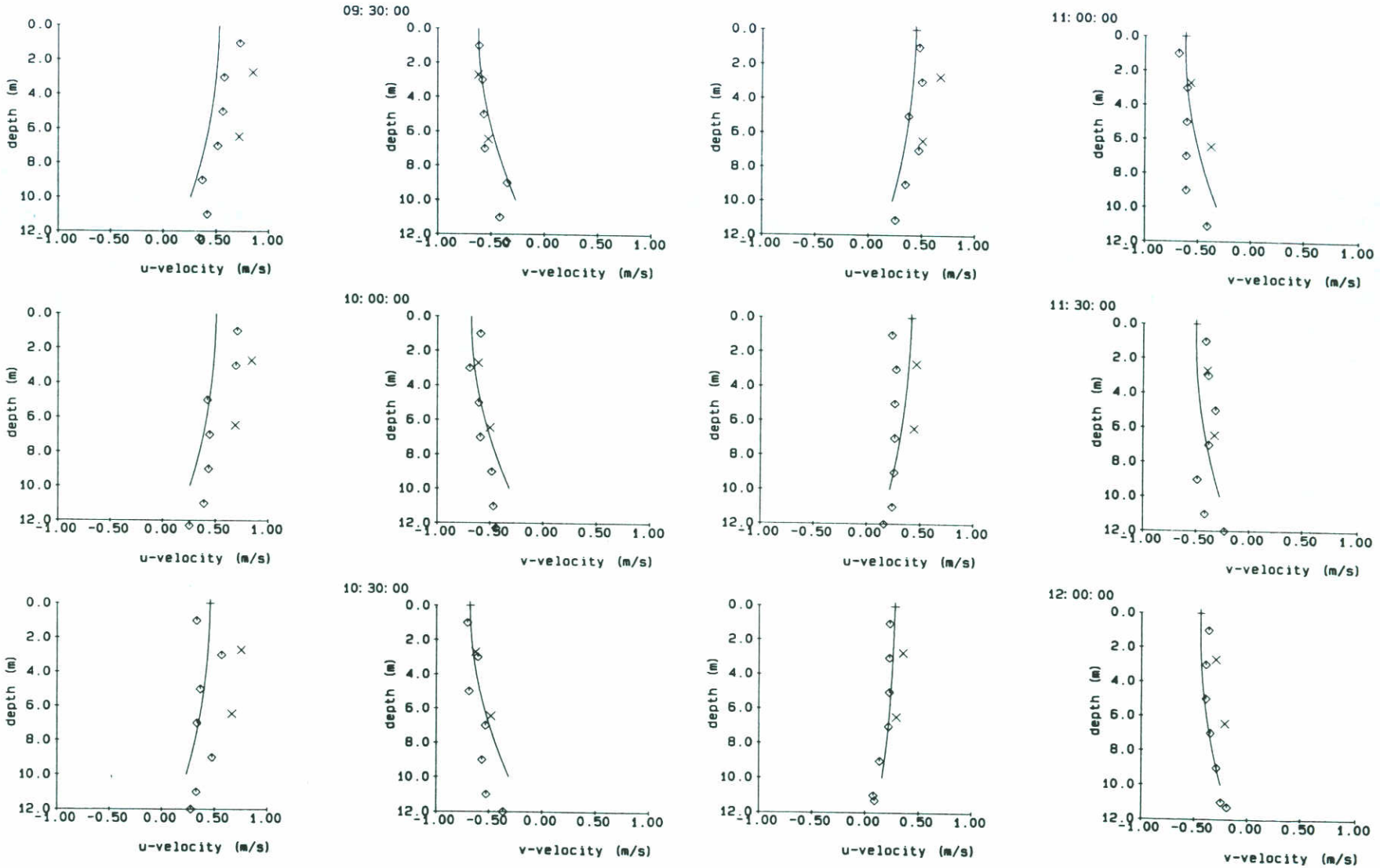

DELFT HYDRAULICS

CURRENT VELOCITY
HF6

VERSIE 1.1

14-11-90

H 972

FIG. 9b

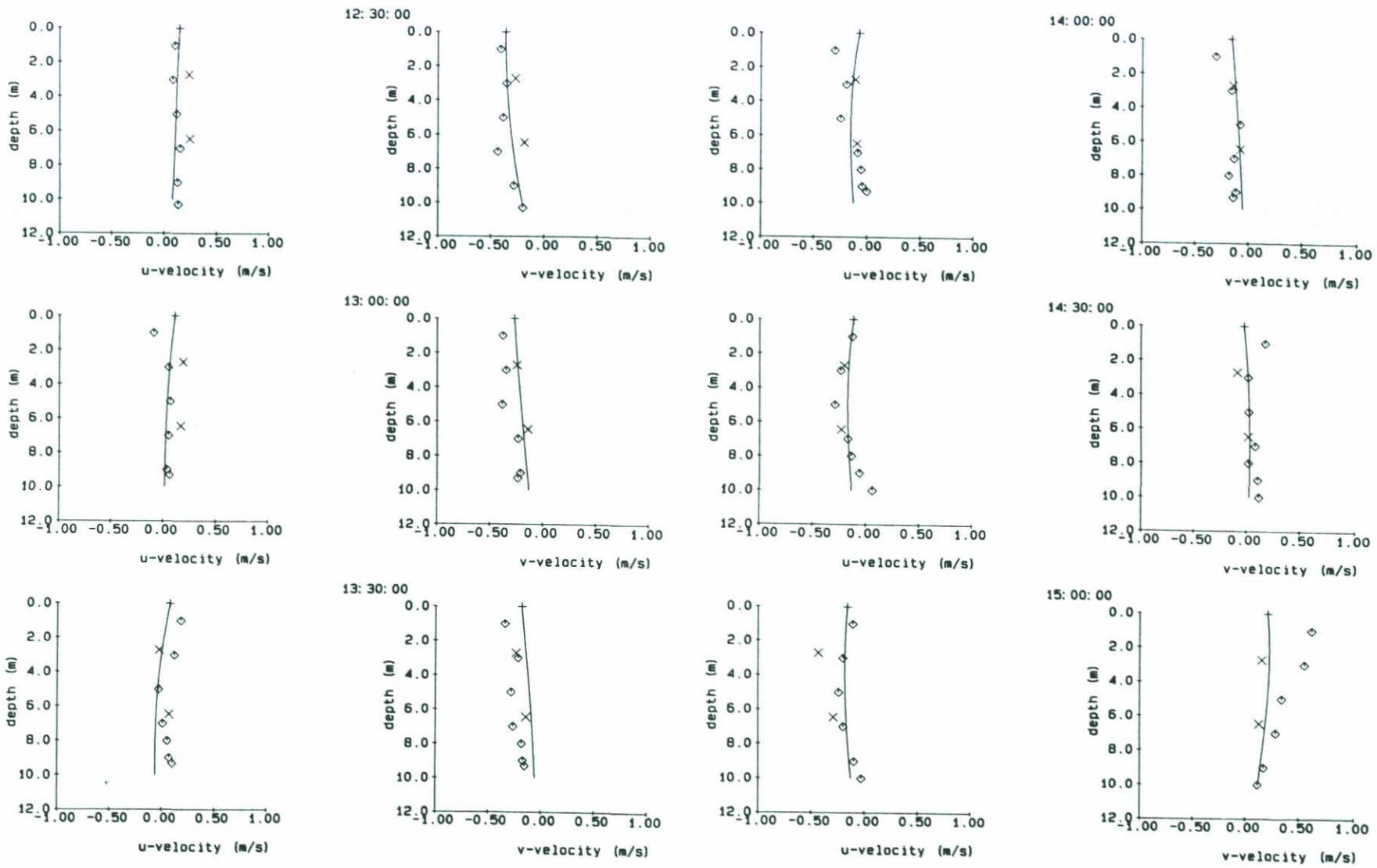

DELFT HYDRAULICS

CURRENT VELOCITY
HF6

H 972 | VERSIE 1.1 | 14-11-90

FIG. 9c

88-11-17

15: 30: 00

16: 00: 00

16: 30: 00

17: 00: 00

17: 30: 00

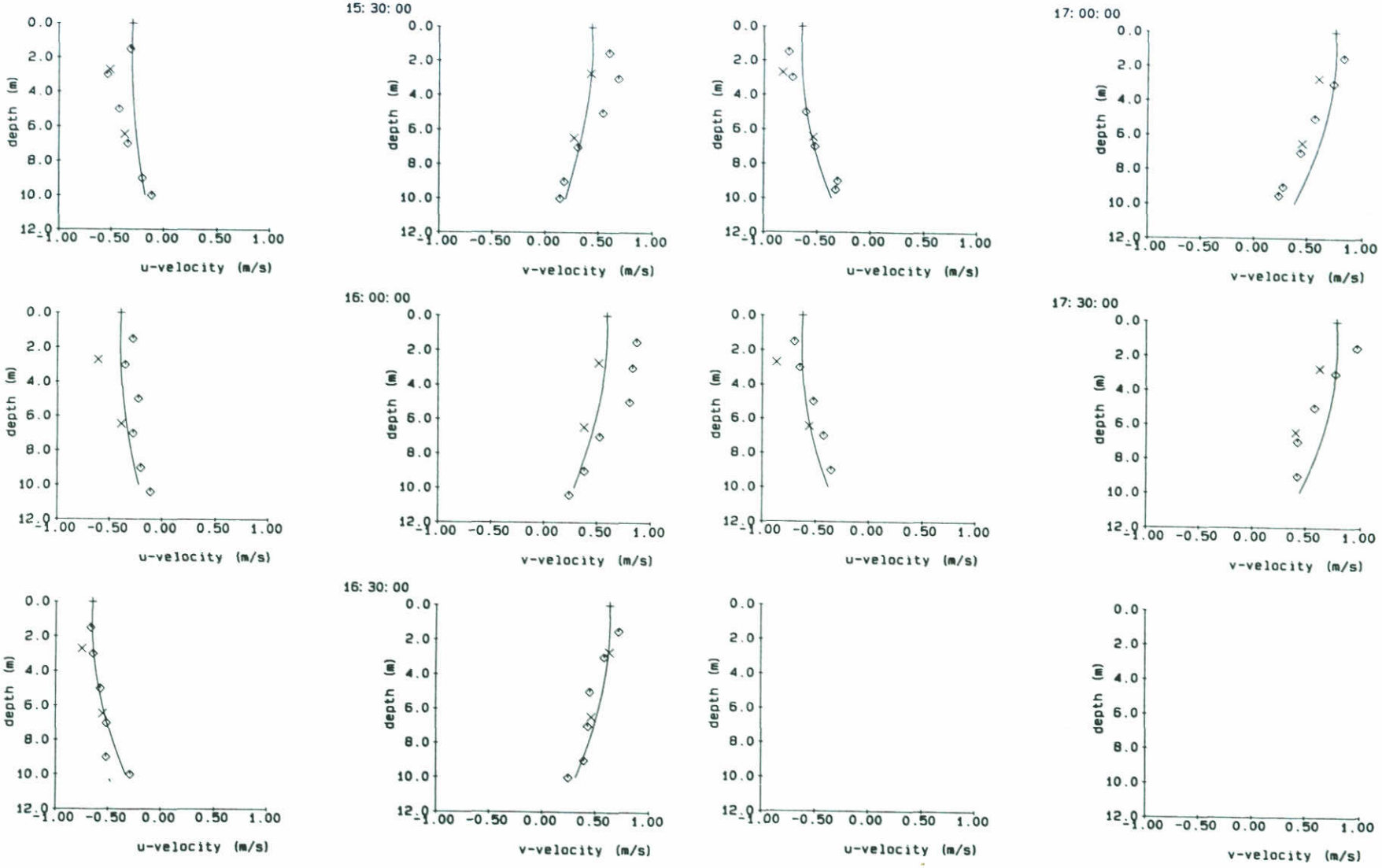

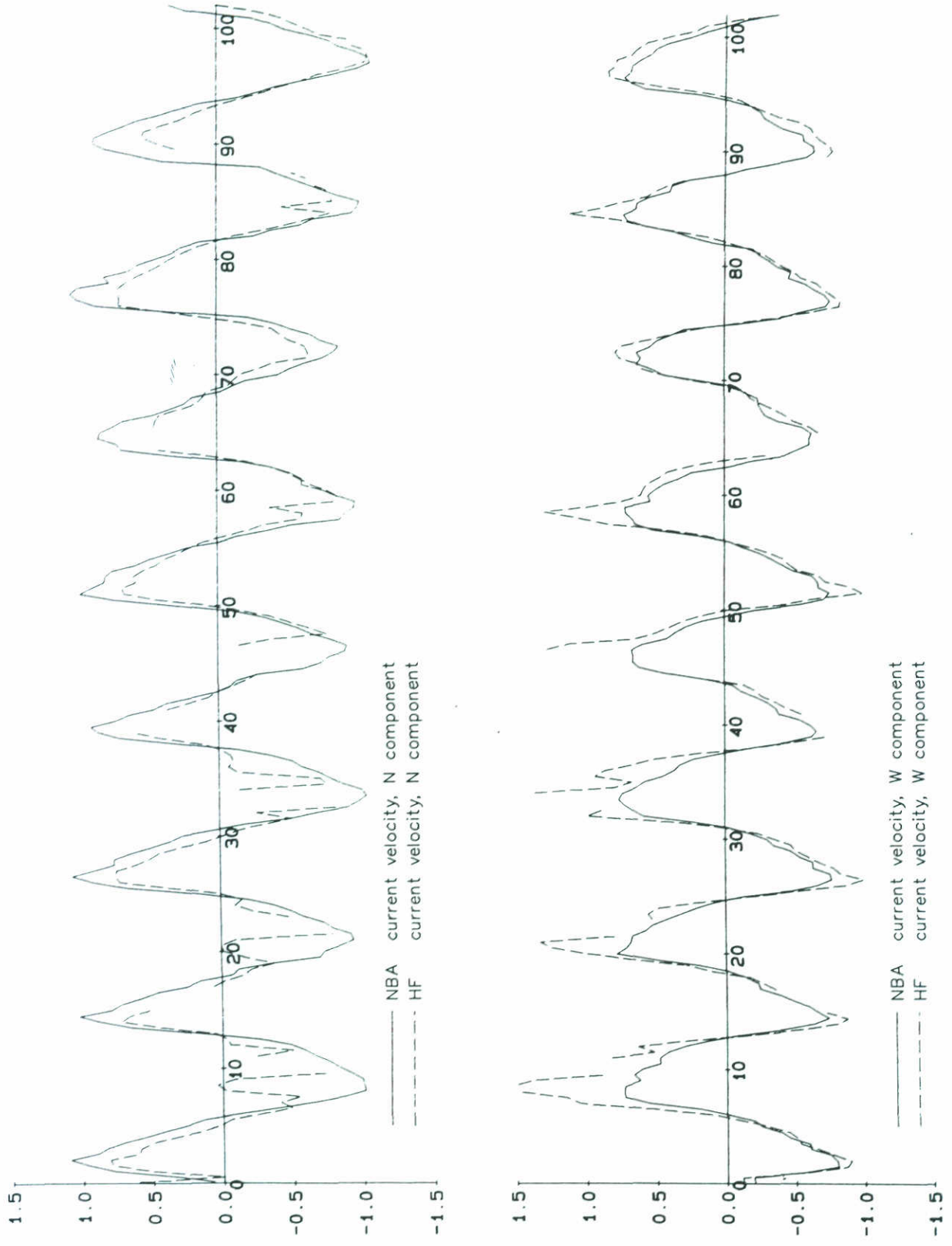

14-11-1800 to 18-11-2330 7.30 m.

DELFT HYDRAULICS | H 972 | FIG. 10

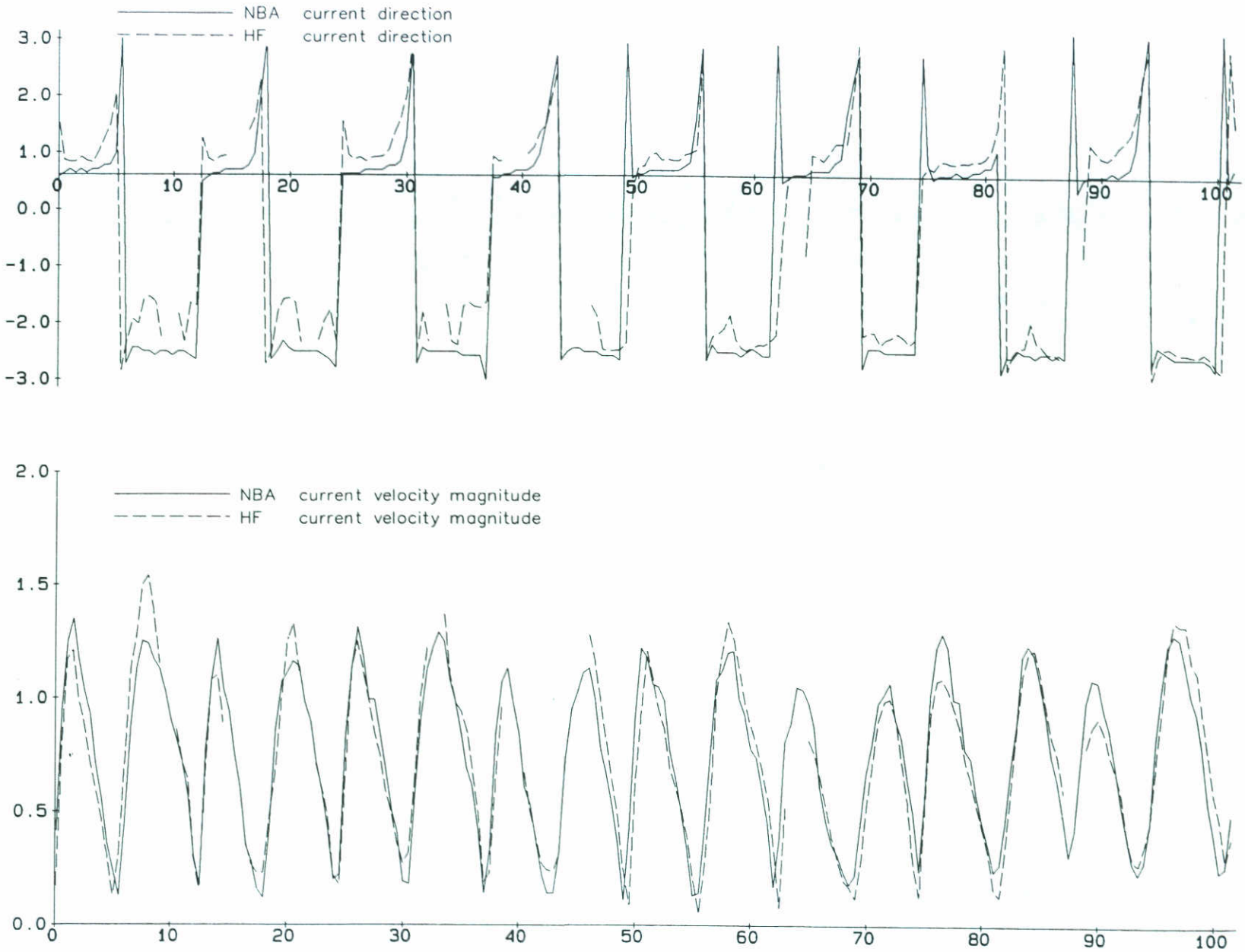

DELFT HYDRAULICS

14-11-1800 to 18-11-2330 7.30 m.

H 972

FIG. 11

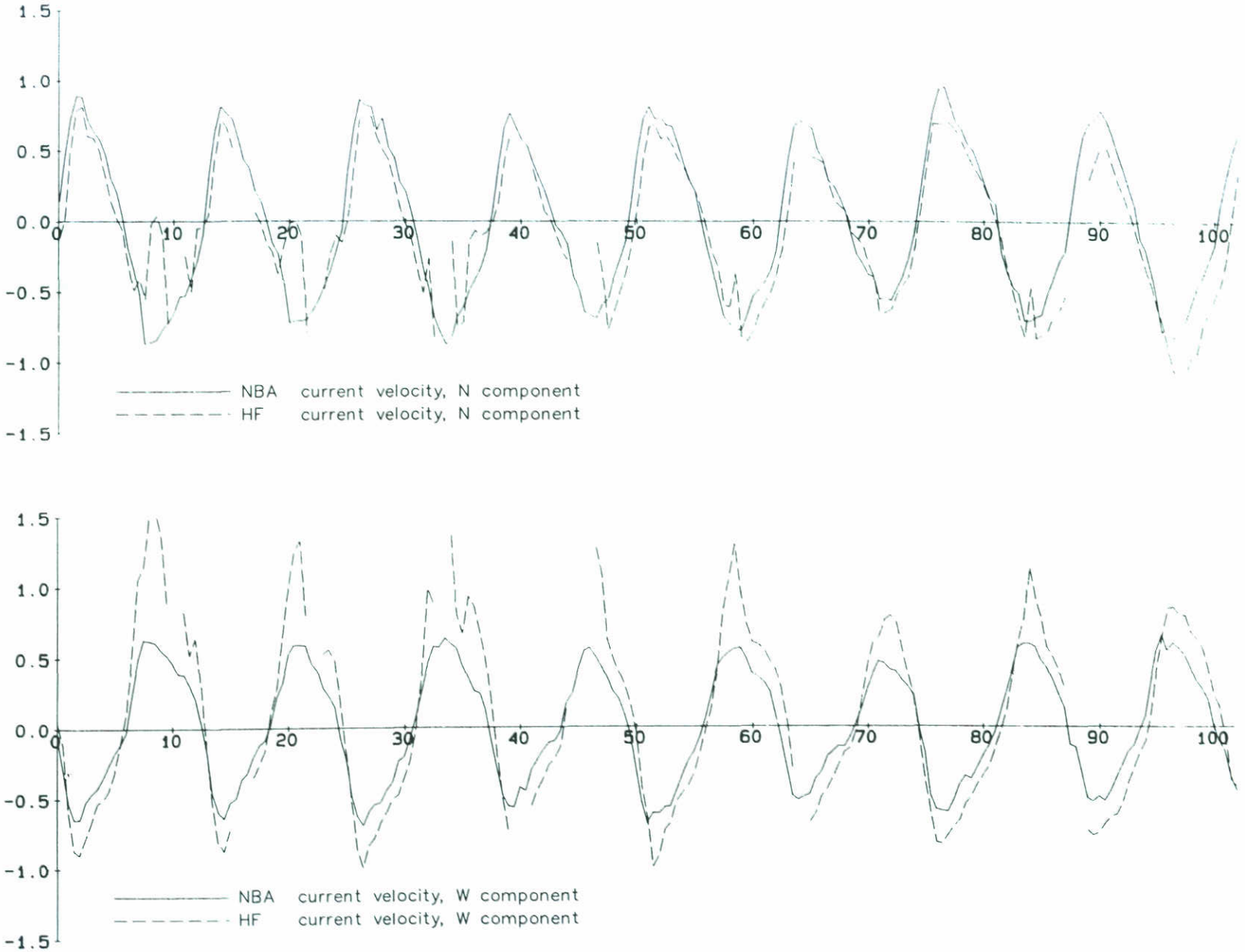

DELFT HYDRAULICS

14-11-1800 to 18-11-2330

3.55 m.

H 972

FIG. 12

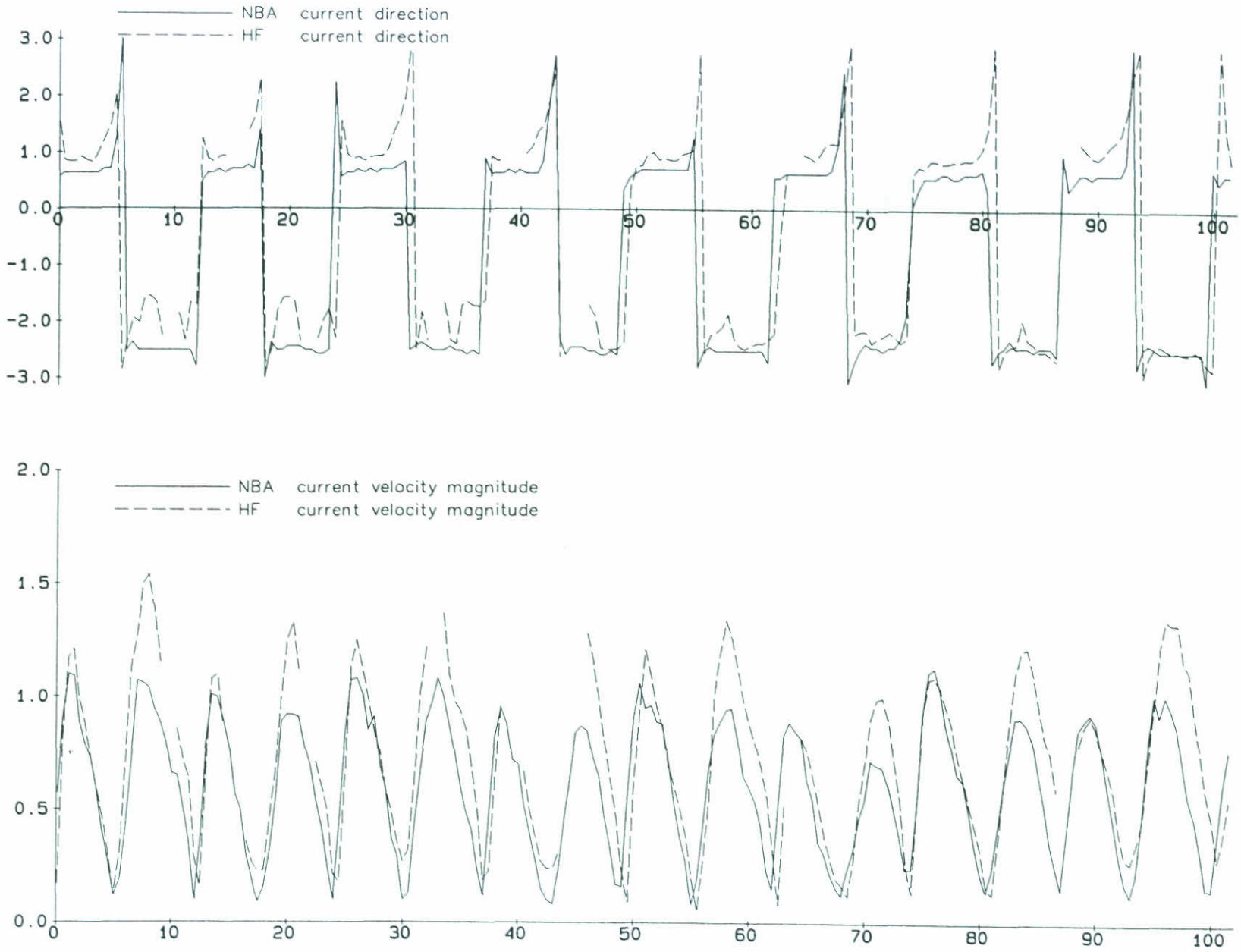

DELFT HYDRAULICS

14-11-1800 to 18-11-2330 3.55 m.

H 972

FIG. 13

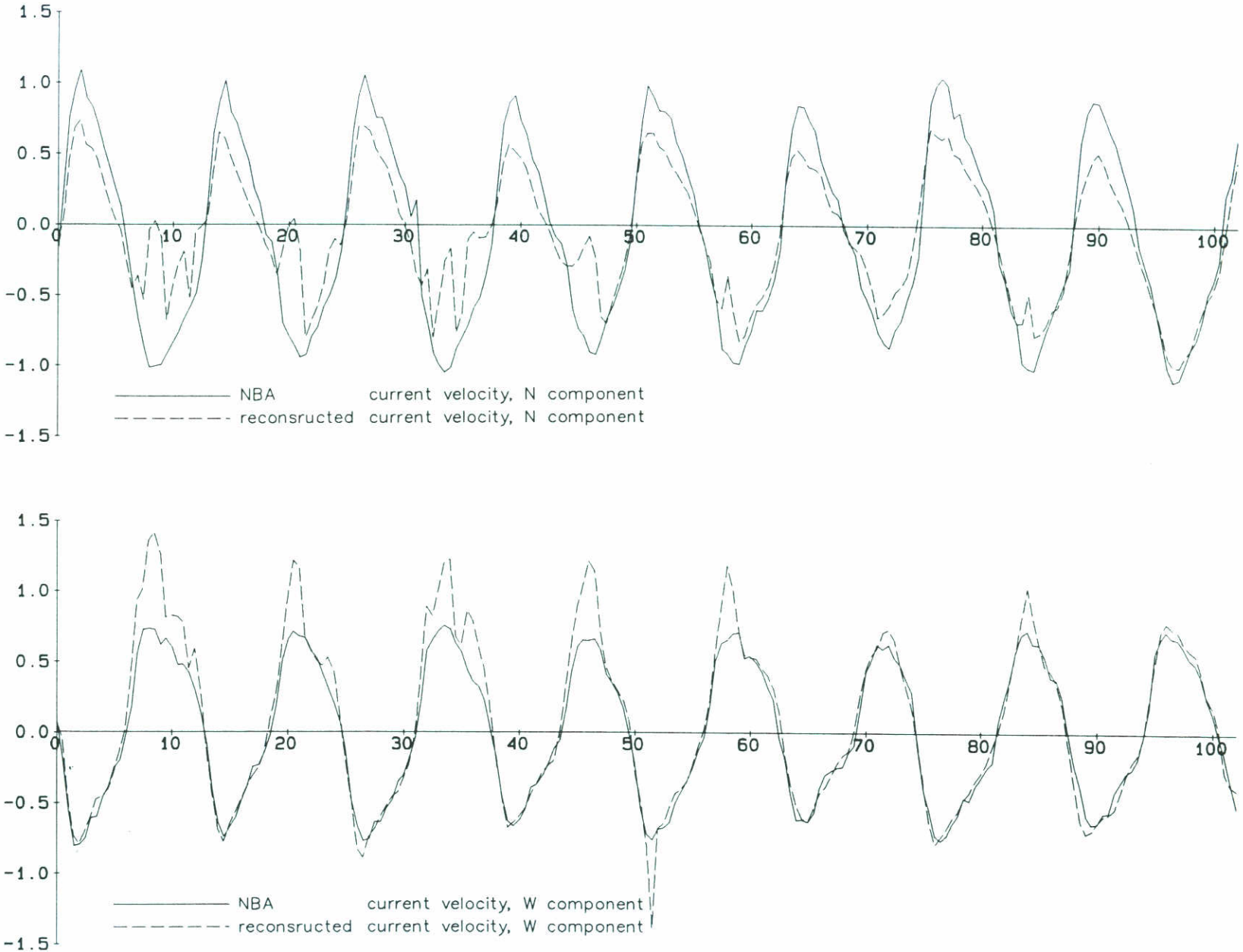

14-11-1800 to 18-11-2330 7.30 m.

DELFT HYDRAULICS

H 972

FIG. 14

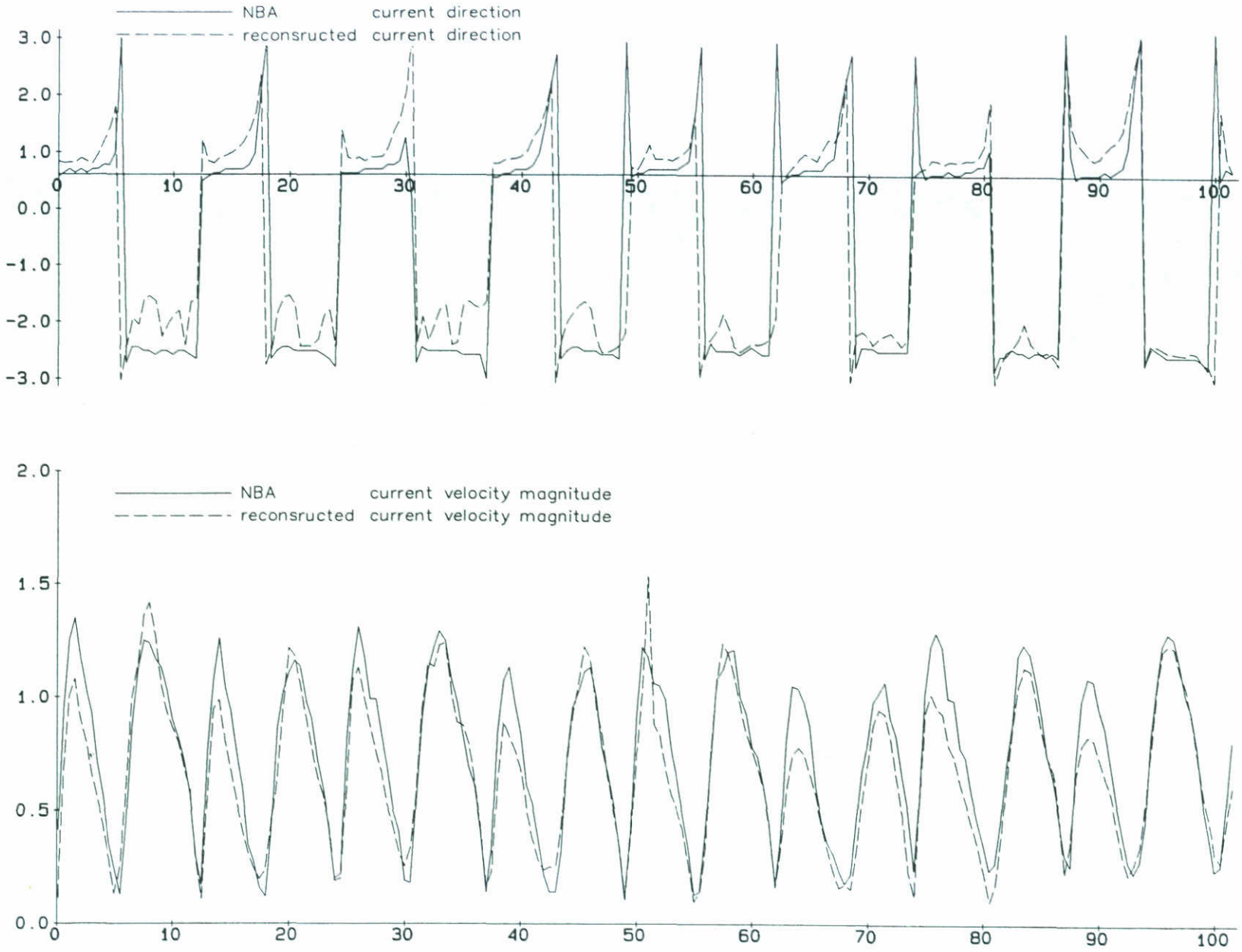

14-11-1800 to 18-11-2330 7.30 m.

DELFT HYDRAULICS

H 972

FIG. 15

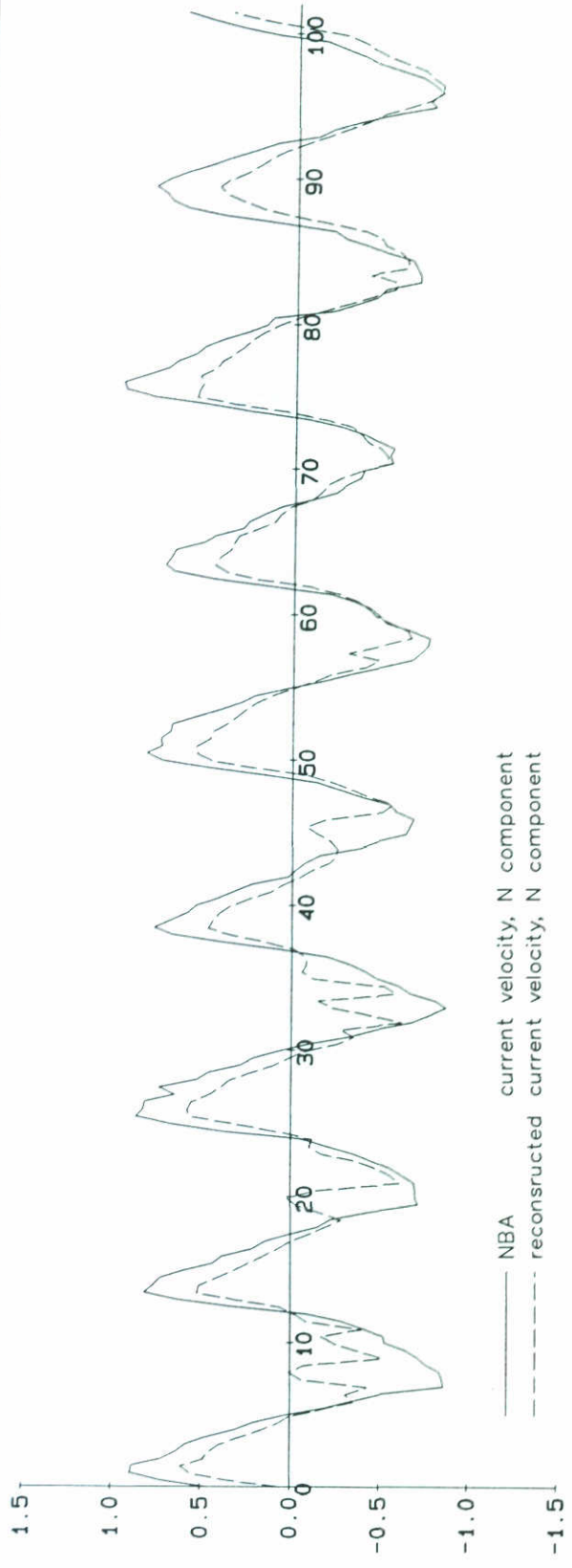

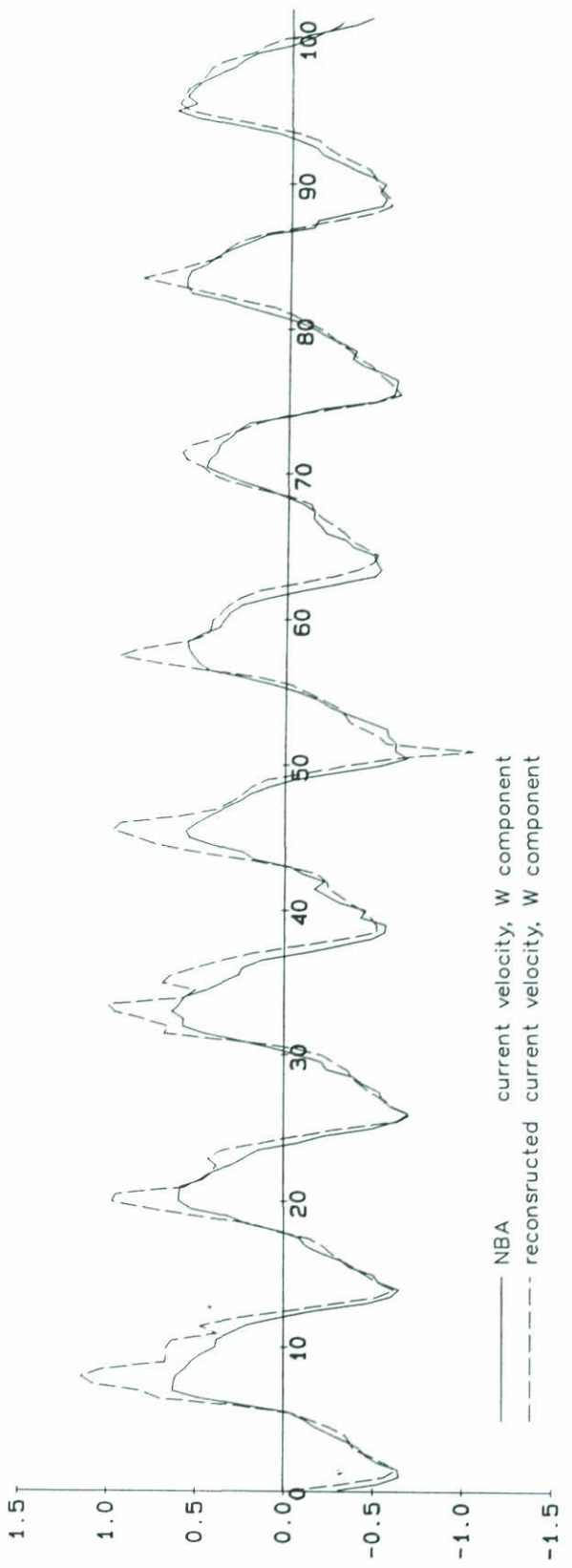

14-11-1800 to 18-11-2330 3.55 m.

DELFT HYDRAULICS | H 972 | FIG. 16

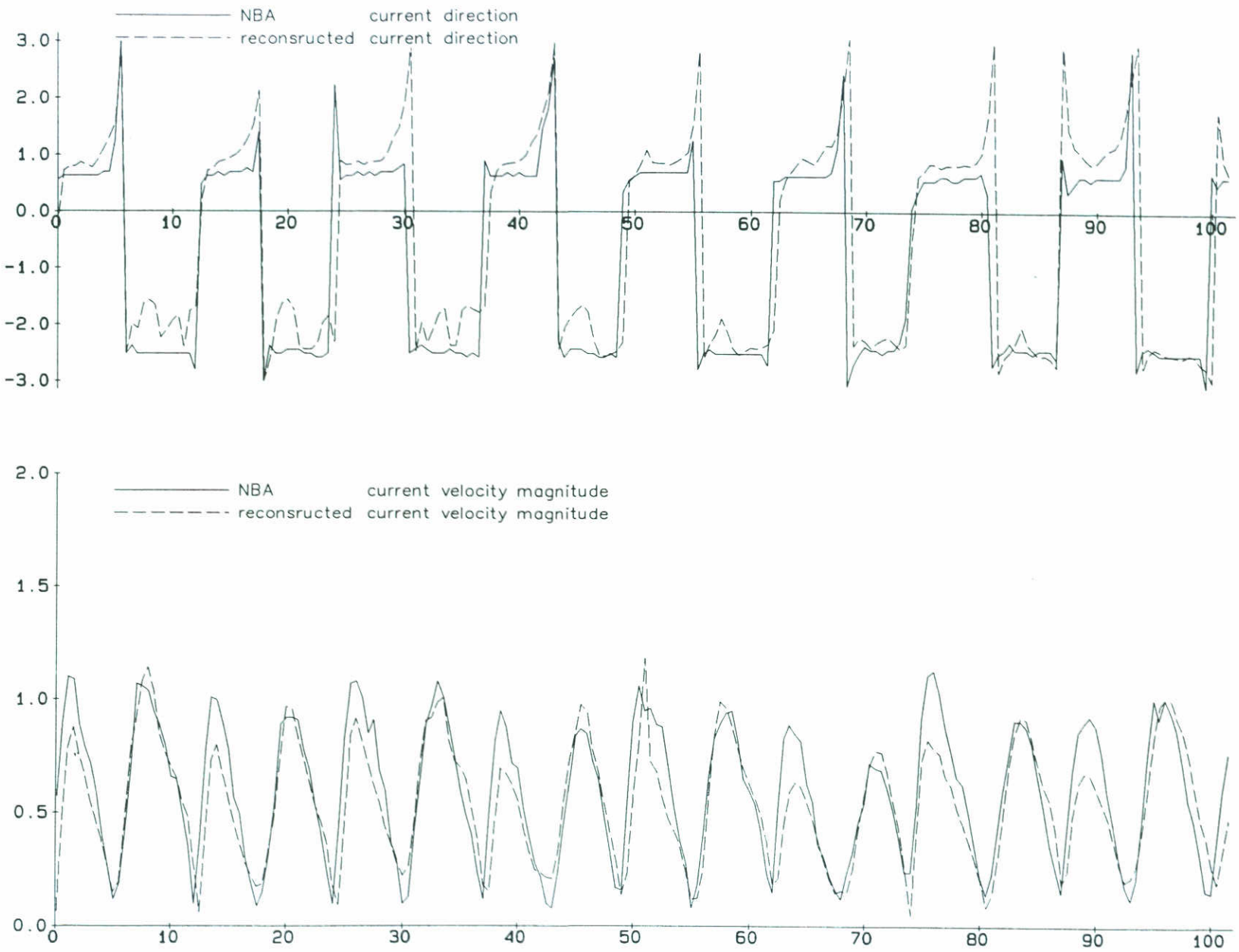

DELFT HYDRAULICS

14-11-1800 tc 18-11-2330 3.55 m.

H 972

FIG. 17

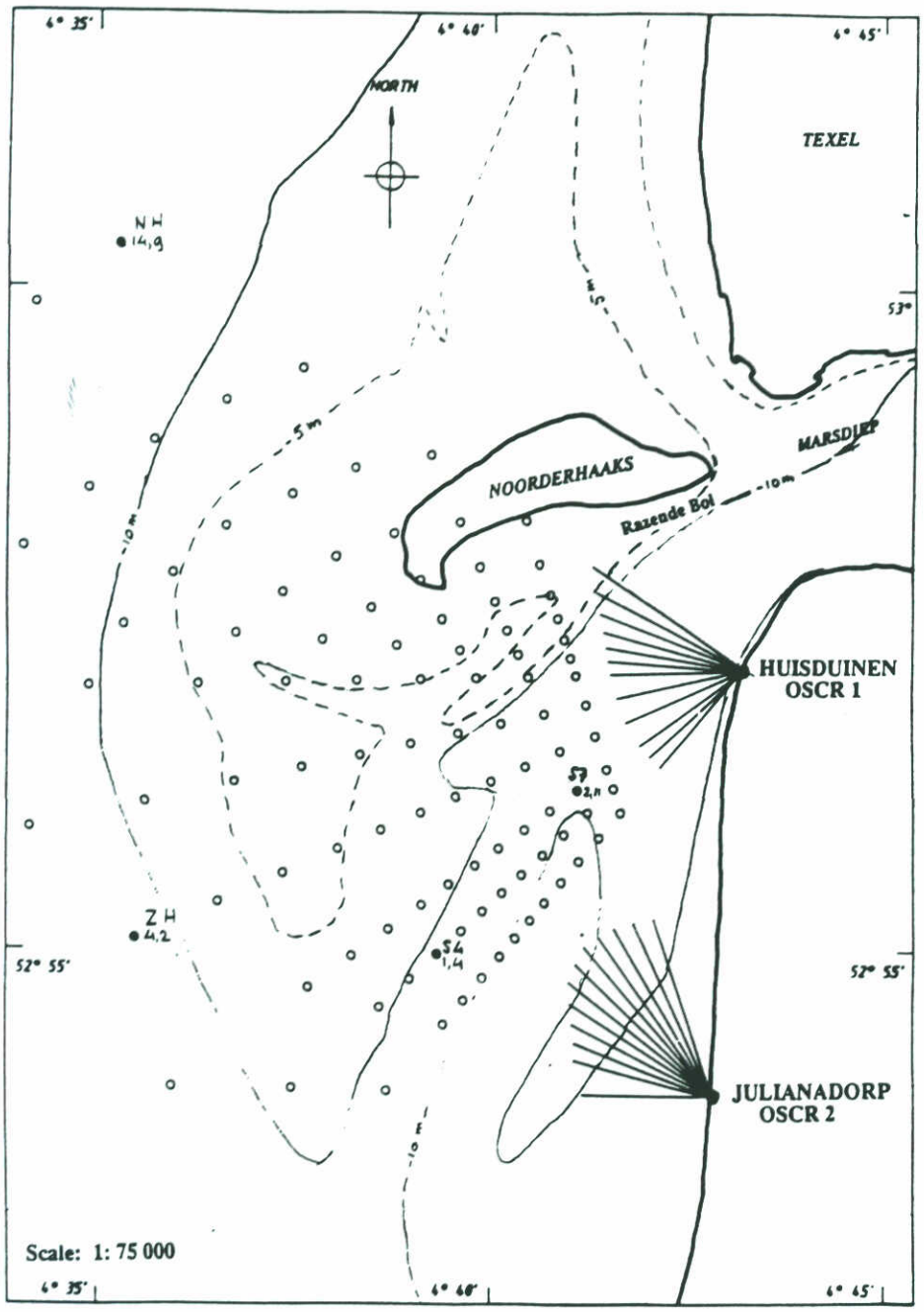

SITUATION SKETCH HF RADAR EXPERIMENT IN NOORD–HOLLAND. CIRCLES ARE HF RADAR MEASUREMENTS LOCATIONS (FROM RIJKSWATERSTAAT (1990))		
DELFT HYDRAULICS	H 972	FIG. 18

main office
Rotterdamseweg 185
p.o. box 177
2600 MH Delft
The Netherlands
telephone (31) 15 - 56 93 53
telefax (31) 15 - 61 96 74
telex 38176 hydel-nl

location ' De Voorst'
Voorsterweg 28, Marknesse
p.o. box 152
8300 AD Emmeloord
The Netherlands
telephone (31) 5274 - 29 22
telefax (31) 5274 - 35 73
telex 42290 hylvo-nl